Report

Cell Reports

A tRNA-Derived Small RNA Regulates Ribosomal Protein S28 Protein Levels after Translation Initiation in Humans and Mice

Graphical Abstract

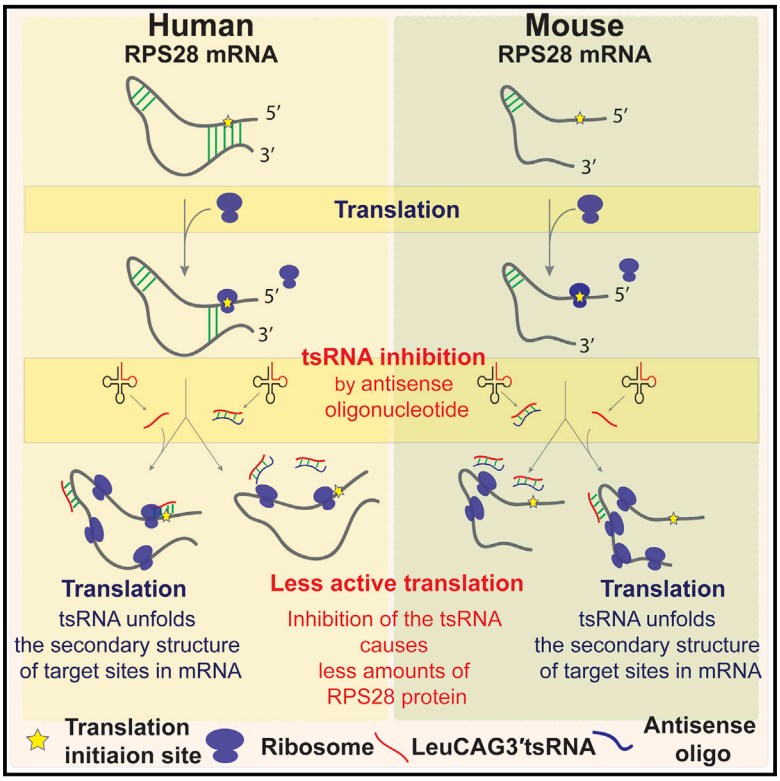

Highlights

- LeuCAG3′tsRNA target site in the *RPS28* coding sequence is conserved in vertebrates
- LeuCAG3′tsRNA regulates *RPS28* translation after the initiation step in humans and mice
- LeuCAG3′tsRNA-regulated translation is conserved between humans and mice
- tsRNA-regulated translational mechanism might be conserved among vertebrates

Authors

Hak Kyun Kim, Jianpeng Xu, Kirk Chu, ..., Paul N. Valdmanis, Qiangfeng Cliff Zhang, Mark A. Kay

Correspondence

markay@stanford.edu

In Brief

Kim et al. determined that the LeuCAG3′tsRNA target site in the *RPS28* coding sequence (CDS) is conserved in vertebrates and established that the tsRNA regulation of RPS28 mRNA translation is conserved between humans and mice. Their results suggest that the tsRNA-regulated mRNA translation might be a conserved process.

Kim et al., 2019, Cell Reports *29*, 3816–3824
December 17, 2019
https://doi.org/10.1016/j.celrep.2019.11.062

CellPress

OPEN ACCESS
CellPress

Cell Reports
Report

A tRNA-Derived Small RNA Regulates Ribosomal Protein S28 Protein Levels after Translation Initiation in Humans and Mice

Hak Kyun Kim,[1,2,5] Jianpeng Xu,[1,2] Kirk Chu,[1,2] Hyesuk Park,[1,2] Hagoon Jang,[1,2] Pan Li,[3] Paul N. Valdmanis,[4] Qiangfeng Cliff Zhang,[3] and Mark A. Kay[1,2,6,*]

[1]Department of Pediatrics, Stanford University, Stanford, CA 94305, USA
[2]Department of Genetics, Stanford University, Stanford, CA 94305, USA
[3]MOE Key Laboratory of Bioinformatics, Beijing Advanced Innovation Center for Structural Biology, Center for Synthetic and Systems Biology, Tsinghua-Peking Joint Center for Life Sciences, School of Life Sciences, Tsinghua University, Beijing 100084, China
[4]Division of Medical Genetics, Department of Medicine, University of Washington, Seattle, WA 98195, USA
[5]Department of Life Science, Chung-Ang University, Seoul 156-756, Republic of Korea
[6]Lead Contact
*Correspondence: markay@stanford.edu
https://doi.org/10.1016/j.celrep.2019.11.062

SUMMARY

tRNA-derived small RNAs (tsRNAs) have been implicated in many cellular processes, yet the detailed mechanisms are not well defined. We previously found that the 3′ end of Leu-CAG tRNA-derived small RNA (LeuCAG3′tsRNA) regulates ribosome biogenesis in humans by maintaining ribosomal protein S28 (RPS28) levels. The tsRNA binds to coding (CDS) and non-coding 3′ UTR sequence in the *RPS28* mRNA, altering its secondary structure and enhancing its translation. Here we report that the functional 3′ UTR target site is present in primates while the CDS target site is present in many vertebrates. We establish that this tsRNA also regulates mouse *Rps28* translation by interacting with the CDS target site. We further establish that the change in mRNA translation occurred at a post-initiation step in both species. Overall, our results suggest that LeuCAG3′tsRNA might maintain ribosome biogenesis through a conserved gene regulatory mechanism in vertebrates.

INTRODUCTION

Historically, the central dogma has been that tRNAs recognize the mRNA triplet sequence on a ribosome to deliver the appropriate amino acid to a growing polypeptide chain. There is a growing appreciation that mature tRNAs alter gene expression in a more complex manner (Schimmel, 2018). tRNAs are differentially expressed in various cancers, tissues, and developmental stages. Each tRNA has an average of eleven to thirteen post-transcriptional modifications, which can affect tRNA folding and function. The tRNA-interacting enzymes potentially add complexity to their various functions. Furthermore, there is increasing evidence that tRNA-derived small RNAs (tsRNAs) (Haussecker et al., 2010), also called tRNA fragments (tRFs) (Lee et al., 2009), affect many cellular processes such as cell proliferation, apoptosis, global translation inhibition, epigenetic inheritance, and neuronal function (Kumar et al., 2016a; Schimmel, 2018). To date, more than six subtypes have been identified based on their cleavage site and length. The longer forms, 30- to 40- nt tsRNAs, are produced by angiogenin-mediated cleavage in the anti-codon loop of mature tRNA and are called tiRNA (tRNA-derived stress-induced RNA) (Yamasaki et al., 2009). The shorter forms, 18- to 26-nt tsRNAs, are somewhat similar to microRNAs (miRNAs) in terms of their length. However, they are not processed by Dicer and the microprocessor complex required for microRNA biogenesis (Haussecker et al., 2010; Kumar et al., 2014; Lee et al., 2009; Li et al., 2012).

One of the known roles for tsRNAs is to regulate mRNA translation by non-canonical mechanisms. In mammalian cells, the 5′ tiRNAs represses global translation by displacing translation eukaryotic initiation factor eIF4A and eIF4G from mRNAs (Guzzi et al., 2018; Ivanov et al., 2011). tiRNA-regulated translation is also observed in other organisms, including *Haloferax volcanii* and *Trypanosoma brucei*. However, the mechanisms of regulation differ among species (Fricker et al., 2019; Gebetsberger et al., 2012).

Distinct from the global translation-inhibitory effects of tsRNAs or tiRNAs, we recently discovered that a specific small non-coding RNA derived from the 3′ end of the Leu-CAG tRNA (LeuCAG3′tsRNA) maintains the translation of *RPS28* (ribosomal protein S28) mRNAs and ultimately the number of ribosomes (Figure S1A) (Kim et al., 2017). RPS28 is a component of the 40S ribosome and is essential for the biogenesis of 18S rRNA (Robledo et al., 2008). Inhibition of LeuCAG3′tsRNA reduces *RPS28* mRNA translation, resulting in reduced 18S rRNA processing and lower numbers of 40S ribosomal subunits. LeuCAG3′tsRNA inhibition leads to apoptosis in human cancer cells and an orthotopic hepatocellular carcinoma (HCC) patient-derived xenograft (PDX) model in mice (Kim et al., 2017; Slack, 2018).

Mechanistically, the LeuCAG3′tsRNA binds to two target sites in human *RPS28* mRNA and disrupts the secondary structure of both target sites: target A in the coding sequence (CDS) and target B in the 3′ UTR enhancing mRNA translation (Figures S1A and S1B). Target A in the CDS forms a local hairpin structure, while target B in the 3′ UTR forms a duplex with a 20-nt

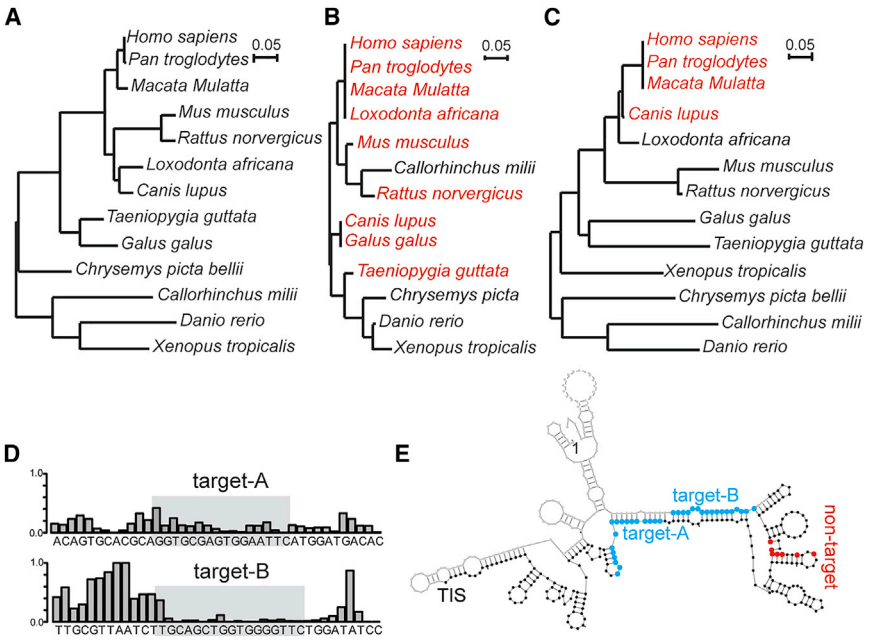

Figure 1. The Target A Site of Leu-CAG3′tsRNA in the *RPS28* CDS Region Is Conserved in Mammals and Birds, and the Two Target Sites in Mouse *Rps28* mRNA Have a Double-Stranded Secondary Structure

(A–C) Phylogenetic trees of 13 vertebrate species based upon their *RPS28* mRNA sequence (A), target A site sequence in the *RPS28* CDS region (B), and target B site sequence in the *RPS28* 3′ UTR (C). The branch length is proportional to the number of changes that have occurred in each species. The species that have predicted human LeuCAG3′tsRNA target sites are colored red (B and C).

(D) The icSHAPE data track the LeuCAG3′tsRNA binding sites in the mouse *Rps28* mRNA. The icSHAPE data are scaled from 0 (no reactivity; double-strandedness) to 1 (maximum reactivity; single-strandedness). The gray box represents the target site. The complete icSHAPE data for mouse *Rps28* mRNA are in Table S2.

(E) Schematic of the mouse *Rps28* mRNA (NM_001355384.1) secondary structure predicted based on the icSHAPE analysis. Blue, the potential binding sites of the LeuCAG3′tsRNA; red, the modified nucleotide of the non-target *Rps28* mutant; TIS, translation initiation site.

region that straddles the translation initiation site (TIS) (Figure S1B) (Kim et al., 2017). This made it difficult to determine the step at which *RPS28* mRNA translation was regulated. To establish the mechanism by which this tsRNA enhances the translation of its target mRNAs, we sought to predict the Leu-CAG3′tsRNA target sites in *RPS28* mRNAs across various vertebrate species and use this information to delineate the process by which the non-coding RNA regulates translation.

RESULTS

Target Site Conservation in the RPS28 mRNA for Vertebrate Species

We determined 22 nt of the 3′ end of the Leu-CAG tRNA in 44 vertebrate species from the Genomic tRNA Database (http://gtrnadb2009.ucsc.edu) and calculated the genetic distances (p distances) between species (Nei and Kumar, 2000). The p distance (0.198) was low, indicating that the LeuCAG3′tsRNA sequence was nearly identical across the tested species. This result was also confirmed by the 95%–100% identity of the mature LeuCAG3′tsRNA for thirteen representative vertebrate species in which the LeuCAG3′tsRNA sequence was identical or differed by just 1 nt (Figure S1C).

To determine the conservation of the LeuCAG3′tsRNA target sites in *RPS28* mRNA for vertebrates, we built a phylogenetic tree of full-length *RPS28* mRNA sequences from thirteen representative vertebrate species (Figure 1A) and predicted the potential targets of LeuCAG3′tsRNA in the *RPS28* mRNA based on the intermolecular minimal free energy (m.f.e.) (Figure S1D). We found two major target sites, one in the CDS and the other in the 3′ UTR, from the many vertebrate species and generated the phylogenetic trees for both potential target sites (Figures 1B and 1C). The predicted nucleotide sequence making up the target A site in the CDS is nearly identical in mammals and birds (Figures 1B and S1D). We also examined the target A site in 100 vertebrate species by comparing an average of phyloP conservation scores of 22-nt sliding windows across the entire *RPS28* CDS (Figure S1E). This analysis showed that the average conservation score of a group of seven 22-nucleotide windows spanning the target A site was ranked second among all seven grouped 22-nt windows spanning the entire *RPS28* CDS, suggesting selective pressure to preserve the conserved tsRNA target site for 100 vertebrate species.

In contrast to the target A site, the target B site in the 3′ UTR is present only in some mammals, such as non-human primates and dogs (Figures 1C and S1D). We next asked whether target B in 3′ UTR forms a double-stranded secondary structure with the translation initiation site (TIS) in the chimpanzee, rhesus monkey, and dog (Figures S1F–S1H) like the human (Figure S1B), using the RNAfold program (Hofacker and Stadler, 2006). The chimpanzee and rhesus monkey, but not the dog, were predicted to have the correct target B secondary structure to interact with the TIS (Figures S1F–S1H). This structure prediction suggests that only primates might have a functional target B site regulating *RPS28* mRNA translation. The lack of the functional target B site in non-primate species raised the question of whether LeuCAG3′tsRNA enhances *RPS28* mRNA translation and, if yes, whether it does so by solely unfolding the target A site in the CDS.

Both Target Sites of LeuCAG3′tsRNA in Mouse RPS28 mRNA Are Double Stranded

We elected to investigate tsRNA-mediated *Rps28* mRNA translation in the mouse. There are two *Rps28* isoforms that differ by 4 nt in the 3′ UTR. Only transcript 2 (NM_001355384.1) is transcribed in the liver (Table S1) (Valdmanis et al., 2016) and is the

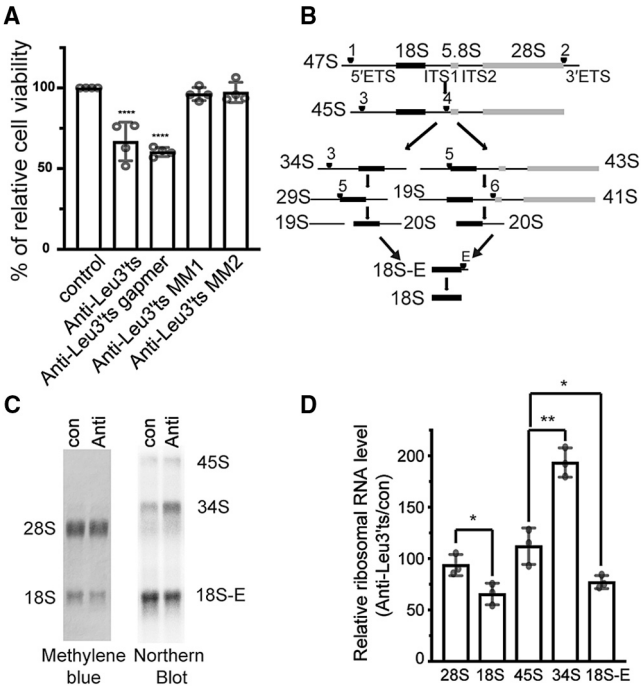

Figure 2. LeuCAG3′tsRNA Is Essential and Required for 18S rRNA Processing in Mouse Cells

(A) Inhibition of LeuCAG3′tsRNA impairs Hepa 1–6 cell viability. Three days post-transfection, a MTS assay was performed (n = 4 independent experiments). Anti-Leu3′ts, antisense oligonucleotide to LeuCAG3′tsRNA; anti-Leu3′ts gapmer, antisense oligonucleotide that induces RNase H activity to cleave LeuCAG3′tsRNA; anti-Leu3′ts MM and MM2, two 2-nt mismatched oligonucleotides to LeuCAG3′tsRNA.

(B) Pre-rRNA processing pathways in mouse cells based on prior studies (Bowman et al., 1981; Kent et al., 2009). The 47S primary transcript is processed and categorized as 5′ external transcribed spacers (5′ ETSs), 18S rRNA, internal transcribed spacer 1 (ITS1), 5.8S rRNA, internal transcribed spacer 2 (ITS2), 28S rRNA, and 3′ external transcribed spacers (3′ ETSs). There are two alternative processing pathways. Inhibition of LeuCAG3′tsRNA inhibits processing from the pre-34S to the pre-20S form depicted in pathway A. Arrowhead and number indicate cleavage sites.

(C and D) Inhibition of the LeuCAG3′tsRNA suppresses 5′ ETS processing in 18S rRNA biogenesis in Hepa 1–6 cells. Methylene blue staining (28S and 18S rRNA) and northern hybridization (45S, 34S, and 18S-E pre-rRNA) were performed with total RNA from Hepa 1–6 cells 24 h post-transfection (n = 3 independent experiments). A representative image is shown in (C). Relative mature and pre-rRNA levels are shown in (D). The rRNA level from anti-Leu3′ts-transfected cells was normalized to that from con (control).

The mean is shown in (A) and (D). Error bar, SD. *$p < 0.05$, **$p < 0.005$, ****$p < 0.0001$ by one-way ANOVA (A) and two-tailed t test (D). Anti, anti-LeuCAG3′tsRNA; con, control.

most abundant in other tissues (Brawand et al., 2011); thus, it was selected for further study.

The tsRNA-target A and tsRNA-target B m.f.e. in mice were −23.7 and −24.6 kcal/mol, respectively (Figure S1I), suggesting that the tsRNA might bind to both regions of the mouse *Rps28* mRNA transcript 2. Both targets have a double-stranded confirmation similar to that of the human *RPS28* mRNA based on icSHAPE (*in vivo* click selective 2′-hydroxyl acylation and profiling experiment) data (Figure 1D; Table S2) (Spitale et al., 2015). However, icSHAPE-based or computational structure modeling predicted that the detailed secondary structure models of the tsRNA target sites differed between mouse and human mRNAs (Figures 1E, S1B, and S1J). Specifically, the mouse target B site, in contrast to the human site, does not form a duplex within the region straddling the translation initiation site (TIS) (Figures 1E, S1B, and S1J).

Therefore, our results suggest both the target A and target B sites in the expressed mouse *Rps28* mRNA isoform exist as double-stranded forms in cells, although the nature of the double-stranded regions in the target B sites differs between mouse and human.

Mouse LeuCAG3′tsRNA Is Required for 18S rRNA Processing

Decreasing the RPS28 protein by inhibiting the LeuCAG3′tsRNA impairs the 18S rRNA processing pathway in human cells, ultimately reducing the viability of human cancer cells (Kim et al., 2017). The LeuCAG3′tsRNA sequence is identical between mouse and human and is expressed at similar levels in HeLa (human cervical cancer) cells and Hepa 1–6 cells (mouse hepatoma cells) (Figure S2A). We next confirmed that as in the human (Kim et al., 2017), the anti-Leu3′ts ASO blocked mouse LeuCAG3′tsRNA, but not the cognate mature tRNA, while the scrambled and two 2-nt mismatched ASOs did not affect the tsRNA concentrations (Figure S2B). Similar to human cells (Kim et al., 2017), inhibition of the LeuCAG3′tsRNA significantly reduced Hepa 1–6 cell viability to 66.8% ± 9.3% compared with control (con) cells (Figure 2A).

As in the human, we ruled out direct binding of the ASO with rRNA and the *Rps28* mRNA (Figures S2C and S2D) (Kim et al., 2017). In addition, the specificity of the anti-Leu3′ts ASO that binds to sequester the target RNA was confirmed using an anti-Leu3′ts gapmer ASO that induces RNase H-mediated cleavage of their target RNAs (Figure 2A) (Jepsen et al., 2004; Kim et al., 2017).

As before, the inhibition of LeuCAG3′tsRNA significantly decreased the 18S rRNA level to 65.5% ± 10.5% compared with control cells. In agreement with previous findings (Kim et al., 2017), the 28S rRNA was not significantly reduced (93.7% ± 10.3%), confirming that the LeuCAG3′tsRNA specifically affects the 18S, but not the 28S, rRNA abundance (Figures 2C and 2D). To determine the step of action on 18S rRNA processing, we measured the relative abundance of different 18S pre-rRNAs by northern hybridization (Figures 2B–2D). Inhibition of the LeuCAG3′tsRNA resulted in the accumulation of the 34S pre-rRNA (equivalent to human 30S pre-rRNA) to a level of 193.5% ± 14.3% compared with the level in control cells, while the 18S-E pre-rRNA level decreased to 77.1% ± 6.3% (Figures 2B–2D). However, the 45S primary transcript only slightly increased to 112.1% ± 71% (Figure 2B–2D). Altogether, these results suggest that the LeuCAG3′tsRNA does not affect rRNA transcription but is required for the processing of the 34S intermediate RNA, as was the case in human (Kim et al., 2017). In addition, in both human (Kim et al., 2017; Robledo et al., 2008) and mouse cells, RNAi knockdown of *RPS28* mRNA resulted in a similar reduction in 5′ external transcribed spacer (ETS) rRNA processing (Figures S2E and S2F), suggesting that the RPS28 protein level plays a similar role in ribosome biogenesis in both species.

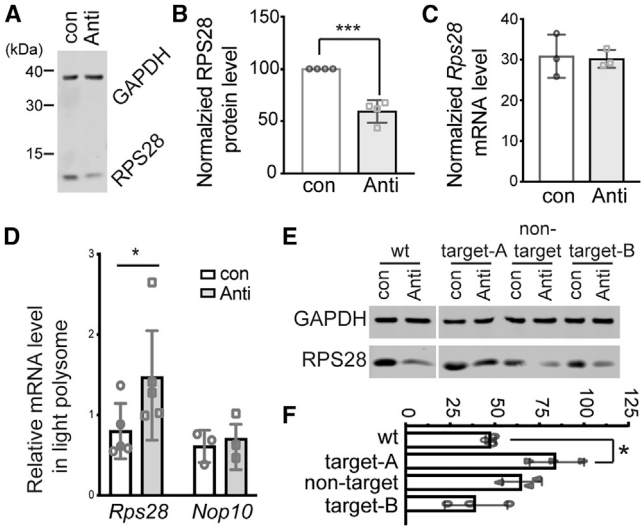

Figure 3. LeuCAG3′tsRNA Is Required for Mouse *Rps28* mRNA Translation through Base Pairing with the Target A Site in the CDS

(A) Representative western blotting image of mouse RPS28 protein from Hepa 1–6 cells 24 h post-transfection (n = 4 independent experiments). GAPDH, loading control.

(B) Average value of four independent experiments shown in (A). The RPS28 protein level was normalized to the Gapdh protein level.

(C) *Rps28* mRNA concentration was determined by real-time PCR 24 h post-transfection and normalized to the *Gapdh* mRNA level (n = 3 independent experiments).

(D) The amount of specific mRNAs in the light polysome (fractions 8 to 10) was normalized to the amount in the heavy polysome (fractions 11 to 13) 24 h post-transfection of ASOs (con, control; anti, anti-Leu3′ts) shown in Figure S3B (n = 3 independent experiments).

(E) A representative western blot result from co-transfection of ASOs and the *Rps28* WT or mutant plasmids (n = 3 independent experiments). The altered target sites or non-target site are indicated in Figure 1E.

(F) The mean value of three independent experiments in (E). The relative RPS28 protein level from each sample was normalized to the GAPDH protein level; subsequently, the calculated relative RPS28 protein level in the anti-Leu3′ts-transfected cells was normalized to the control transfected cells.

The mean is indicated in (B)–(D) and (F). Error bar, SD. *p < 0.05, ***p < 0.0005 by two-tailed t test.

LeuCAG3′tsRNA Regulates Mouse Rps28 mRNA Translation

The RPS28 protein levels (Figures 3A and 3B) and mRNA levels (Figure 3C) were quantified by western blot and real-time PCR, respectively, after the ASO-mediated inhibition of LeuCAG3′tsRNA. Reduction of the active LeuCAG3′tsRNA resulted in a decrease in the RPS28 protein while the mRNA concentration was unchanged, consistent with an effect on translation (Figures 3A–3C). To establish this, we performed sucrose gradient fractionation in LeuCAG3′tsRNA-inhibited cells (Figure S3). As observed in human cells, inhibition of the LeuCAG3′tsRNA caused a decrease in the 18S rRNA level (Figures 2C and 2D), likely resulting in the reduced 40S ribosomal subunit concentration and subsequent lowering of the 80S monosomes (Figure S3A). Next, to determine the polysomal distribution of *Rps28* and two control mRNAs (*Nop10* and *Gapdh*), we extracted total RNA from each fraction across the gradient for northern blot quantification (Figures S3B and S3C). Mouse *Rps28* and *Nop10* coding sequences are 210 and 195 nt, respectively, making their maximal ribosome density similar. Mouse *Rps28* mRNA was most highly represented in fraction 11, indicative of three to four ribosomes per mRNA. Inhibition of LeuCAG3′tsRNA significantly shifted the *Rps28* mRNA into the lighter fractions 8–10, corresponding to two to three ribosomes per mRNA ($p = 0.0492$ in fraction 10, $p = 0.0155$ in fraction 11), while the *Nop10* and *Gapdh* mRNA were primarily found in fractions 11 and 14, respectively, and were not different in both anti-Leu3′ts ASO- and control ASO-treated cells (Figures S3B and S3C). There was no significant change in *Rps28* mRNA concentrations in fractions 6 and 7, where the initiating ribosomes (monosomes) co-migrate. This suggested that translational regulation occurred at a step other than initiation.

To quantify how much *Rps28* mRNA shifted from the heavier fractions (11 to 13) to lighter fractions (8 to 10), we calculated the relative *Rps28* mRNA abundance in the lighter compared with the heavier polysomal fraction from the data shown in Figure S3B. The normalized light fraction contained 0.8 ± 0.34 of the *Rps28* mRNA in wild-type (WT) cells, but this was increased to 1.47 ± 0.68 ($p = 0.0179$) when the LeuCAG3′tsRNA was inhibited. The relative amount of normalized *Nop10* mRNA contained in the lighter fraction was marginally increased from 0.61 ± 0.20 to 0.71 ± 0.28 when the tsRNA was reduced (Figure 3D). These results confirmed that that LeuCAG3′tsRNA regulates *Rps28* mRNA translation in both mouse and human cells.

LeuCAG3′tsRNA-Regulated Mouse Rps28 mRNA Translation Depends on a Target Site in the CDS

The mouse *Rps28* mRNA has two potential LeuCAG3′tsRNA target sites; target A in the CDS and target B in the 3′ UTR (Figure 1E). The target A site sequence is almost identical between mouse and human, but the target B site is not (Figure S1D). In addition, the target B site does not form a duplex with the region straddling the TIS (Figures 1E and S1J). To establish whether the LeuCAG3′tsRNA modulates *Rps28* mRNA translation with the potential target sites in mouse cells, we constructed expression plasmids containing either a wild type (WT) or various *Rps28* mutations (target A, target B, and non-target), which alters mRNA nucleotides, but not the amino acid sequence (Figure 1E). To avoid codon biases that might affect expression, we replaced the codon sequence with those that have comparable codon usage in the *Rps28* mutants. The target A and B mutants were predicted to disrupt the tsRNA-*Rps28* mRNA interaction and therefore abolish the tsRNA regulation of mRNA translation, while the non-target mutants were not expected to affect the tsRNA-mediated translational regulation.

We co-transfected each plasmid with either control (con) or anti-Leu3′ts (anti) ASOs in Hepa 1–6 cells and examined protein expression by western blot analysis (Figures 3E and 3F). Compared with RPS28 protein expression from control cells, the anti-Leu3′ts ASO-mediated inhibition of LeuCAG3′tsRNA reduced the RPS28 protein concentrations from the wild-type and non-target mutant mRNAs to 47.6% ± 2.7% and 64.8% ± 11.1%, respectively, while the protein level derived from the target A mutant (the conserved target) mRNA was minimally decreased to 84.0% ± 15.2% (Figures 3E and 3F). Unlike the target A mutant, the target B mutant (the non-conserved

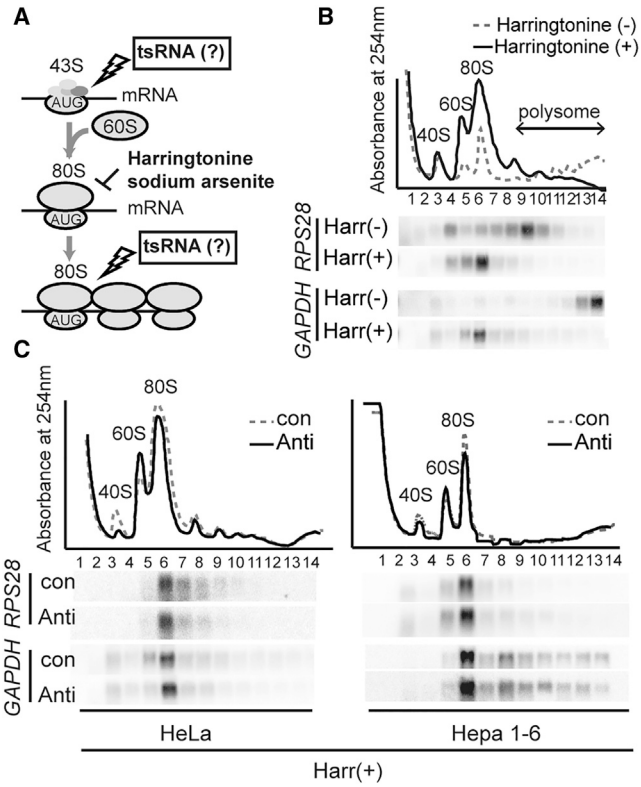

Figure 4. LeuCAG3′tsRNA Regulates Both Human and Mouse *RPS28* Translation in the Elongation Phase

(A) A schematic representation of the possible translation steps affected by the LeuCAG3′tsRNA using harringtonine (B and C) and sodium arsenite (Figures S4B and S4C). If the tsRNA affects 80S complex formation, the harringtonine or sodium arsenite treatments stall *RPS28* mRNA near the 40S subunit (Figure S4A). If the tsRNA affects the step after 80S complex formation, the harringtonine or sodium arsenite treatments stall *RPS28* mRNA on the 80S complex (Figures 4B and S4B).

(B) Harringtonine treatment in HeLa cells (n = 2 independent experiments).

(C) Harringtonine treatment post-transfection in HeLa (left) and Hepa 1–6 (right) cells (n = 2 independent experiments). The polysome profile (top) and northern hybridization (bottom) were analyzed. The polysome profile indicates the position of 40S and 60S ribosomal free subunits, monosomes, and polysomes on each designated fraction.

Harringtonine (+) and Harr(+), treatment with harringtonine; Harringtonine (−) and Harr(-), no treatment with harringtonine; con, control; anti, anti-Leu3′ts.

target) had levels of RPS28 protein 39.1% ± 17.6% of wild-type (Figures 3E and 3F) after tsRNA inhibition, suggesting that the target B site was not active in mouse cells.

Altogether, these results suggest that mouse LeuCAG3′tsRNA regulates mouse *Rps28* mRNA translation primarily using the more conserved target site (target A) in the CDS, while the less conserved sequence (target B) in the 3′ UTR is not used as a regulatory site.

LeuCAG3′tsRNA Regulates RPS28 mRNA Translation at a Post-initiation Step in Humans and Mice

The human LeuCAG3′tsRNA unfolds the secondary structure at both the TIS and the coding sequence (Figure S1B) (Kim et al., 2017), while the mouse *Rps28* mRNA TIS is not functionally active (Figures 1E, 3E, and 3F). As a result, we could not predict whether the tsRNA-based translational enhancement was more likely to occur at the step of initiation or post-initiation and whether these mechanisms were the same or different in humans and mice.

To establish whether a translational initiation block can be discriminated with sucrose gradient fractionation, we used small interfering RNAs (siRNAs) to knock down of *RPL7* and *RPL35A*, which inhibits the production of the 60S subunit and hence the formation of the 80S monosome (Figure S4A). We quantified mRNAs in the various polysomal fractions after sucrose gradient fractionation and found the *RPS28* and *RPS13* mRNAs stall near the 40S ribosomal free subunit (fraction 4), indicating a block in forming new 80S initiation monosome complexes (Figure S4A).

We next treated HeLa and Hepa 1–6 cells with either harringtonine (Figures 4A and 4B) or sodium arsenite (Figures 4A and S4B) and compared *RPS28* and *GAPDH* mRNA sedimentation using sucrose gradient fractionation. Harringtonine prevents the first peptide bond formation (Fresno et al., 1977; Ingolia et al., 2012), and sodium arsenite reduces eukaryotic initiation factor 4E protein levels (Othumpangat et al., 2005) and/or induces the phosphorylation of eukaryotic initiation factor 2α (Kim et al., 2011). Both drugs result in the freezing of the mRNA-ribosome complexes after formation of an 80S monosome while allowing mRNAs in the polysomal fraction to run off (Figures 4B and S4B). Thus, if *RPS28* mRNA translation was being suppressed at the level of post-initiation, the *RPS28* mRNA would co-sediment with the 80S monosome, whereas if initiation is affected, the *RPS28* mRNA would accumulate in the non-polysomal fractions lighter than the 80S monosome (e.g., 40S ribosomal free subunit) (Figures 4A and S4A).

As expected, *RPS*28 and *GAPDH* mRNAs that normally migrated in fractions 9 and 14, respectively, accumulated on the 80S monosome with harringtonine or sodium arsenite (Figures 4B and S4B). Inhibition of LeuCAG3′tsRNA did not change the accumulation of both mRNAs on the 80S monosome complex in cells treated with harringtonine or sodium arsenite (Figures 4C and S4C). Upon treatment with sodium arsenite, the presence of *GAPDH* mRNA at fraction 3 (43S pre-initiation) suggests that this drug also affected formation of the *GAPDH mRNA*-80S monosome complex (Figures S4B and S4C). These results strongly suggest that the LeuCAG3′tsRNA regulates *RPS28* mRNA at the level of post-translation initiation in both species.

To support our model, we also determined whether the LeuCAG3′tsRNA is associated with polysomes (Figure S4D). We determined the migration of a mRNA, two microRNAs, a tRNA, and two tsRNAs in the polysomal fractions of a sucrose gradient. The GAPDH mRNA, miR-92a, Let-7, and mature Leu-CAG tRNAs co-migrated with heavy polysomes (fractions 12–14). Thirty-two percent of the LeuCAG3′tsRNAs migrated with fractions 9–14 (polysomes). In contrast, the LeuCAG5′tsRNA was primarily found in lighter fractions, which contain the free ribonucleoproteins (RNPs) and 40S ribosomal free subunits (fractions 1–3), showing they were not associated with the polysomes. To exclude the binding of LeuCAG3′tsRNAs with other non-polysomal complexes in the gradient, we treated the cells with puromycin, a drug that mimics charged tRNAs and terminates polypeptide chain elongation and release of the polysomes into 40S and 60S subunits. This

also resulted in the release of the mature Leu-CAG tRNAs and LeuCAG3′tsRNA, specifying their association with polysomes in cells (Figure S4D). Altogether, our results strongly support that the LeuCAG3′tsRNA regulates *RPS28* mRNA translation with the target A site at the level of post-initiation in humans and mice. Based on sequence and structure similarities of the target A site, it is highly likely that this mode of regulation is conserved for mammals and possibly vertebrates.

DISCUSSION

Ribosome biogenesis is a complex yet precisely regulated cellular process. Dysregulation of ribosome biogenesis or abnormal expression of ribosomal proteins (RPs) is associated with disease states such as Treacher Collins syndrome (TCS), Shwachman-Bodian-Diamond syndrome (SBDS), dyskeratosis congenita, $5q^-$ syndrome, and Diamond-Blackfan anemia (DBA) (Freed et al., 2010; Sulima et al., 2017). In fact, a *RPS28* mutation in TCS/MFD (mandibulofacial dysostosis) and DBA patients has been reported (Gripp et al., 2014). In addition, augmented ribosome biogenesis plays a role in various malignant processes (Bywater et al., 2013; Pelletier et al., 2018).

The importance of the RPS28 protein in translation can be inferred from its localization to the head of the small ribosomal subunit, where it contacts the 18S rRNA and mRNA near or in the exit E site (Fortier et al., 2015; Pisarev et al., 2008; Robledo et al., 2008). A ribosome that lacks RPS28 might have a detrimental effect on translation, making cell death a preferred outcome in humans and mice. As a result, the precise regulatory processes have likely evolved to regulate the production of this protein. It has been well documented that a decrease in specific ribosomal proteins (RPs) downregulates other RP levels and rRNA processing (Robledo et al., 2008), suggesting that multiple regulatory mechanisms could be in play to fine-tune the production of a subset or all ribosomal proteins.

Here, we predicted and then experimentally were able to demonstrate that the LeuCAG3′tsRNA-regulated *RPS28* mRNA translation in both mouse and human cells. Based on sequence similarities, we predict that similar mechanisms might be operative in other vertebrates, but this will require additional experimentation.

We also demonstrated that the tsRNA regulated translation at the post-initiation step in humans and mice. The most likely post-initiation step regulated by this tsRNA is elongation. While translational initiation is well established for regulating the rates of translation (Kudla et al., 2009; Salis et al., 2009), there is growing evidence suggesting elongation can also play important roles in regulating protein synthesis (Chu et al., 2014; Firczuk et al., 2013). So far, many factors have been identified to affect translation elongation-GC (guanine-cytosine) content, length and structure of the 5′ UTR, codon optimization and/or rare codons, miRNA targets, and secondary structure. Our finding adds to a growing layer of regulatory processes likely required to maintain precise protein concentrations in cells.

The generation and function of multiple types of tsRNAs remain largely unknown. Moreover, quantifying their concentration within cells and tissues is complicated, because most tRNAs have an average of 11–13 modifications per gene (Phizicky and Hopper, 2010). For example, sequencing paradigms often identify 18-nt 3′ tsRNAs rather than the more predominant 22-nt isoform detected by northern hybridization (Kim et al., 2017; Kumar et al., 2015; Li et al., 2012). This is due to the presence of the N1-methyl-adenosine modification conserved at the 58th nt in the TΨC loop (Saikia et al., 2010), which inhibits reverse transcriptase (Findeiss et al., 2011; Renda et al., 2001), a required step for high-throughput sequencing. Even though AlkB-facilitated RNA de-methylation sequencing was recently developed (Cozen et al., 2015; Liu et al., 2016), it warrants more precise sequencing to overcome various tRNA modifications.

Emerging data revealed that the tRNA modifications affect tRNA stability and function, as well as tsRNA expression profiles. m^5C_{38} (m^5C at the C38 position) of Asp, Gly, and Val tRNAs is modified by DNMT2, a multi-substrate tRNA methyltransferase (Lyko, 2018). Disruption of *Dnmt2*-regulated m^5C_{38} also altered the secondary structure of tsRNAs and their stability against RNase degradation (Zhang et al., 2018). Pseudouridine (Ψ) is one of the most abundant modifications in the RNA world (Charette and Gray, 2000). PUS7-mediated Ψ of 5′ tsRNA in human embryonic stem cells activates 5′ terminal oligoguanine (TOG)-containing, tsRNA-mediated global translation inhibition (Guzzi et al., 2018). The 22-nt 3′ tsRNAs also contain modifications, including m^1A_{58} and Ψ, suggesting that these modifications might affect the biogenesis and/or structure and/or function, including the binding of the LeuCAG3′tsRNA with its target. In addition, it is not yet known whether the 3′ end is amino-acylated, a parameter that may affect the biogenesis and/or specific function. All of these findings warrant more investigation on the modification and biogenesis of 3′ tsRNAs.

There are still many unresolved questions about how these tsRNAs regulate translation. First, a potential seed region might be important in the interaction of the tsRNA and target mRNA. Indeed, the last 3 nt of the 3′ canonical end (CCA) of LeuCAG3′tsRNA do not bind to the *Rps28* mRNA (Figure S1I), whereas the importance of the 3′ end of other non-3′ tsRNAs for the interaction with specific targets is noted (Wang et al., 2013; Zhou et al., 2017). Thus, the lack of the CCA interaction with the target might allow greater functional diversity across all 3′ tsRNAs. Second, the importance of the location of the anti-target site and the structure or sequence of the surrounding regions is not known. Lastly, how tsRNA binding influences other parameters known to influence translation is unclear.

Our observation shows that two species have the same function of LeuCAG3′tsRNA, which strongly increases the likelihood that other tsRNAs might disrupt or unwind secondary structures of other mRNAs during translation and that the tsRNAs may have co-evolved with their targets to fine-tune the production of specific proteins, many of which may be involved in protein synthesis. In addition, rRNA, ribosomal proteins (RPs), associated proteins, or modifying proteins may result in ribosome heterogeneity, which may in turn regulate specialized translation of specific transcripts, providing an additional layer to complex gene regulation during cell differentiation and organismal development (Genuth and Barna, 2018).

We demonstrated that the LeuCAG3′tsRNA enhances RPS28 protein synthesis in humans and mice, and more recently, Luo

et al. (2018) found that non-3′ tsRNAs repress ribosomal protein expressions in *Drosophila*, suggesting that varied tsRNAs might be important *de novo* factors for regulating ribosome biogenesis in various species (Kim et al., 2017).

In addition, our results highlight a potential explanation for why at least some mRNA levels do not necessarily correlate with protein levels (Vogel and Marcotte, 2012; Wilhelm et al., 2014). Further delineating the biogenesis of the more than 150 unique 3′ tsRNAs in mammals, as well as their RNA targets, and their detailed mechanistic functions may reveal an overarching regulatory circuit for fine-tuning gene expression.

STAR★METHODS

Detailed methods are provided in the online version of this paper and include the following:

- KEY RESOURCES TABLE
- LEAD CONTACT AND MATERIALS AVAILABILITY
- EXPERIMENTAL MODEL AND SUBJECT DETAILS
- METHOD DETAILS
  - Transfection
  - Oligonucleotides
  - Plasmid constructs
  - Western blotting
  - Real time PCR
  - RNA isolation and Northern blotting
  - Polysome gradient and RNA preparation
  - The abundance of Rps28 transcript variants in mouse liver tissue
  - Structure probing of tsRNA targets and mouse Rps28 mRNA secondary structure prediction
  - tsRNA target prediction
  - Genetic distances of LeuCAG3′tsRNA
  - Percent identity
  - Sequence alignment of RPS28 sequences
  - Conservation analysis of LeuCAG3′tsRNA target site
- QUANTIFICATION AND STATISTICAL ANALYSIS
- DATA AND CODE AVAILABILITY

SUPPLEMENTAL INFORMATION

Supplemental Information can be found online at https://doi.org/10.1016/j.celrep.2019.11.062.

ACKNOWLEDGMENTS

This work was supported by grants to M.A.K. from the National Institutes of Health, National Institute of Diabetes and Digestive and Kidney Diseases (R01DK114483).

AUTHOR CONTRIBUTIONS

H.K.K. designed experiments; performed experiments, data collection, and interpretation; and wrote the manuscript. J.X. performed bioinformatics analysis. K.C. and H.P. performed experiments. P.L. performed and supplied raw icSHAPE data. P.N.V. performed the RNA-seq studies of *Rps28* transcripts in mouse liver. C.Z. performed and interpretation of the raw icSHAPE data. M.A.K. designed experiments, performed data interpretation, and wrote the manuscript. All authors provided edits and signed off on the final manuscript.

DECLARATION OF INTERESTS

The authors declare no competing interests.

Received: April 22, 2019
Revised: September 3, 2019
Accepted: November 14, 2019
Published: December 17, 2019

REFERENCES

Bowman, L.H., Rabin, B., and Schlessinger, D. (1981). Multiple ribosomal RNA cleavage pathways in mammalian cells. Nucleic Acids Res. *9*, 4951–4966.

Brawand, D., Soumillon, M., Necsulea, A., Julien, P., Csárdi, G., Harrigan, P., Weier, M., Liechti, A., Aximu-Petri, A., Kircher, M., et al. (2011). The evolution of gene expression levels in mammalian organs. Nature *478*, 343–348.

Burland, T.G. (2000). DNASTAR's Lasergene sequence analysis software. Methods Mol. Biol. *132*, 71–91.

Bywater, M.J., Pearson, R.B., McArthur, G.A., and Hannan, R.D. (2013). Dysregulation of the basal RNA polymerase transcription apparatus in cancer. Nat. Rev. Cancer *13*, 299–314.

Chan, P.P., and Lowe, T.M. (2016). GtRNAdb 2.0: an expanded database of transfer RNA genes identified in complete and draft genomes. Nucleic Acids Res. *44* (*D1*), D184–D189.

Charette, M., and Gray, M.W. (2000). Pseudouridine in RNA: what, where, how, and why. IUBMB Life *49*, 341–351.

Chu, D., Kazana, E., Bellanger, N., Singh, T., Tuite, M.F., and von der Haar, T. (2014). Translation elongation can control translation initiation on eukaryotic mRNAs. EMBO J. *33*, 21–34.

Cozen, A.E., Quartley, E., Holmes, A.D., Hrabeta-Robinson, E., Phizicky, E.M., and Lowe, T.M. (2015). ARM-seq: AlkB-facilitated RNA methylation sequencing reveals a complex landscape of modified tRNA fragments. Nat. Methods *12*, 879–884.

Darty, K., Denise, A., and Ponty, Y. (2009). VARNA: Interactive drawing and editing of the RNA secondary structure. Bioinformatics *25*, 1974–1975.

Findeiss, S., Langenberger, D., Stadler, P.F., and Hoffmann, S. (2011). Traces of post-transcriptional RNA modifications in deep sequencing data. Biol. Chem. *392*, 305–313.

Firczuk, H., Kannambath, S., Pahle, J., Claydon, A., Beynon, R., Duncan, J., Westerhoff, H., Mendes, P., and McCarthy, J.E. (2013). An *in vivo* control map for the eukaryotic mRNA translation machinery. Mol. Syst. Biol. *9*, 635.

Fortier, S., MacRae, T., Bilodeau, M., Sargeant, T., and Sauvageau, G. (2015). Haploinsufficiency screen highlights two distinct groups of ribosomal protein genes essential for embryonic stem cell fate. Proc. Natl. Acad. Sci. USA *112*, 2127–2132.

Freed, E.F., Bleichert, F., Dutca, L.M., and Baserga, S.J. (2010). When ribosomes go bad: diseases of ribosome biogenesis. Mol. Biosyst. *6*, 481–493.

Fresno, M., Jiménez, A., and Vázquez, D. (1977). Inhibition of translation in eukaryotic systems by harringtonine. Eur. J. Biochem. *72*, 323–330.

Fricker, R., Brogli, R., Luidalepp, H., Wyss, L., Fasnacht, M., Joss, O., Zywicki, M., Helm, M., Schneider, A., Cristodero, M., and Polacek, N. (2019). A tRNA half modulates translation as stress response in *Trypanosoma brucei*. Nat. Commun. *10*, 118.

Gebetsberger, J., Zywicki, M., Künzi, A., and Polacek, N. (2012). tRNA-derived fragments target the ribosome and function as regulatory non-coding RNA in *Haloferax volcanii*. Archaea *2012*, 260909.

Genuth, N.R., and Barna, M. (2018). The Discovery of Ribosome Heterogeneity and Its Implications for Gene Regulation and Organismal Life. Mol. Cell *71*, 364–374.

Gripp, K.W., Curry, C., Olney, A.H., Sandoval, C., Fisher, J., Chong, J.X., Pilchman, L., Sahraoui, R., Stabley, D.L., and Sol-Church, K.; UW Center for Mendelian Genomics (2014). Diamond-Blackfan anemia with mandibulofacial

dystostosis is heterogeneous, including the novel DBA genes TSR2 and RPS28. Am. J. Med. Genet. A. *164A*, 2240–2249.

Guzzi, N., Cieśla, M., Ngoc, P.C.T., Lang, S., Arora, S., Dimitriou, M., Pimková, K., Sommarin, M.N.E., Munita, R., Lubas, M., et al. (2018). Pseudouridylation of tRNA-Derived Fragments Steers Translational Control in Stem Cells. Cell *173*, 1204–1216.e26.

Haussecker, D., Huang, Y., Lau, A., Parameswaran, P., Fire, A.Z., and Kay, M.A. (2010). Human tRNA-derived small RNAs in the global regulation of RNA silencing. RNA *16*, 673–695.

Hofacker, I.L., and Stadler, P.F. (2006). Memory efficient folding algorithms for circular RNA secondary structures. Bioinformatics *22*, 1172–1176.

Ingolia, N.T., Brar, G.A., Rouskin, S., McGeachy, A.M., and Weissman, J.S. (2012). The ribosome profiling strategy for monitoring translation *in vivo* by deep sequencing of ribosome-protected mRNA fragments. Nat. Protoc. *7*, 1534–1550.

Ivanov, P., Emara, M.M., Villen, J., Gygi, S.P., and Anderson, P. (2011). Angiogenin-induced tRNA fragments inhibit translation initiation. Mol. Cell *43*, 613–623.

Jepsen, J.S., Sørensen, M.D., and Wengel, J. (2004). Locked nucleic acid: a potent nucleic acid analog in therapeutics and biotechnology. Oligonucleotides *14*, 130–146.

Karolchik, D., Hinrichs, A.S., Furey, T.S., Roskin, K.M., Sugnet, C.W., Haussler, D., and Kent, W.J. (2004). The UCSC Table Browser data retrieval tool. Nucleic Acids Res. *32*, D493–D496.

Kent, T., Lapik, Y.R., and Pestov, D.G. (2009). The 5′ external transcribed spacer in mouse ribosomal RNA contains two cleavage sites. RNA *15*, 14–20.

Kim, J.H.J., Park, S.M.S., Park, J.H.J., Keum, S.J.S., and Jang, S.K.S. (2011). eIF2A mediates translation of hepatitis C viral mRNA under stress conditions. EMBO J. *30*, 2454–2464.

Kim, H.K., Fuchs, G., Wang, S., Wei, W., Zhang, Y., Park, H., Roy-Chaudhuri, B., Li, P., Xu, J., Chu, K., et al. (2017). A transfer-RNA-derived small RNA regulates ribosome biogenesis. Nature *552*, 57–62.

Krüger, J., and Rehmsmeier, M. (2006). RNAhybrid: microRNA target prediction easy, fast and flexible. Nucleic Acids Res. *34*, W451–W454.

Kudla, G., Murray, A.W., Tollervey, D., and Plotkin, J.B. (2009). Coding-sequence determinants of gene expression in *Escherichia coli*. Science *324*, 255–258.

Kumar, P., Anaya, J., Mudunuri, S.B., and Dutta, A. (2014). Meta-analysis of tRNA derived RNA fragments reveals that they are evolutionarily conserved and associate with AGO proteins to recognize specific RNA targets. BMC Biol. *12*, 78.

Kumar, P., Mudunuri, S.B., Anaya, J., and Dutta, A. (2015). tRFdb: a database for transfer RNA fragments. Nucleic Acids Res. *43*, D141–D145.

Kumar, P., Kuscu, C., and Dutta, A. (2016a). Biogenesis and Function of Transfer RNA-Related Fragments (tRFs). Trends Biochem. Sci. *41*, 679–689.

Kumar, S., Stecher, G., and Tamura, K. (2016b). MEGA7: Molecular Evolutionary Genetics Analysis Version 7.0 for Bigger Datasets. Mol. Biol. Evol. *33*, 1870–1874.

Lee, Y.S., Shibata, Y., Malhotra, A., and Dutta, A. (2009). A novel class of small RNAs: tRNA-derived RNA fragments (tRFs). Genes Dev. *23*, 2639–2649.

Li, Z., Ender, C., Meister, G., Moore, P.S., Chang, Y., and John, B. (2012). Extensive terminal and asymmetric processing of small RNAs from rRNAs, snoRNAs, snRNAs, and tRNAs. Nucleic Acids Res. *40*, 6787–6799.

Liu, F., Clark, W., Luo, G., Wang, X., Fu, Y., Wei, J., Wang, X., Hao, Z., Dai, Q., Zheng, G., et al. (2016). ALKBH1-Mediated tRNA Demethylation Regulates Translation. Cell *167*, 816–828.e16.

Luo, S., He, F., Luo, J., Dou, S., Wang, Y., Guo, A., and Lu, J. (2018). *Drosophila* tsRNAs preferentially suppress general translation machinery via antisense pairing and participate in cellular starvation response. Nucleic Acids Res. *46*, 5250–5268.

Lyko, F. (2018). The DNA methyltransferase family: a versatile toolkit for epigenetic regulation. Nat. Rev. Genet. *19*, 81–92.

Nei, M., and Kumar, S. (2000). Molecular Evolution and Phylogenetics (Oxford University Press).

O'Leary, N.A., Wright, M.W., Brister, J.R., Ciufo, S., Haddad, D., McVeigh, R., Rajput, B., Robbertse, B., Smith-White, B., Ako-Adjei, D., et al. (2016). Reference sequence (RefSeq) database at NCBI: current status, taxonomic expansion, and functional annotation. Nucleic Acids Res. *44* (*D1*), D733–D745.

Othumpangat, S., Kashon, M., and Joseph, P. (2005). Sodium arsenite-induced inhibition of eukaryotic translation initiation factor 4E (eIF4E) results in cytotoxicity and cell death. Mol. Cell. Biochem. *279*, 123–131.

Pelletier, J., Thomas, G., and Volarević, S. (2018). Ribosome biogenesis in cancer: new players and therapeutic avenues. Nat. Rev. Cancer *18*, 51–63.

Phizicky, E.M., and Hopper, A.K. (2010). tRNA biology charges to the front. Genes Dev. *24*, 1832–1860.

Pisarev, A.V., Kolupaeva, V.G., Yusupov, M.M., Hellen, C.U.T., and Pestova, T.V. (2008). Ribosomal position and contacts of mRNA in eukaryotic translation initiation complexes. EMBO J. *27*, 1609–1621.

Renda, M.J., Rosenblatt, J.D., Klimatcheva, E., Demeter, L.M., Bambara, R.A., and Planelles, V. (2001). Mutation of the methylated tRNA(Lys)(3) residue A58 disrupts reverse transcription and inhibits replication of human immunodeficiency virus type 1. J. Virol. *75*, 9671–9678.

Reuter, J.S., and Mathews, D.H. (2010). RNAstructure: software for RNA secondary structure prediction and analysis. BMC Bioinformatics *11*, 129.

Robinson, J.T., Thorvaldsdóttir, H., Winckler, W., Guttman, M., Lander, E.S., Getz, G., and Mesirov, J.P. (2011). Integrative genomics viewer. Nat. Biotechnol. *29*, 24–26.

Robledo, S., Idol, R.A., Crimmins, D.L., Ladenson, J.H., Mason, P.J., and Bessler, M. (2008). The role of human ribosomal proteins in the maturation of rRNA and ribosome production. RNA *14*, 1918–1929.

Saikia, M., Fu, Y., Pavon-Eternod, M., He, C., and Pan, T. (2010). Genome-wide analysis of N1-methyl-adenosine modification in human tRNAs. RNA *16*, 1317–1327.

Salis, H.M., Mirsky, E.A., and Voigt, C.A. (2009). Automated design of synthetic ribosome binding sites to control protein expression. Nat. Biotechnol. *27*, 946–950.

Schimmel, P. (2018). The emerging complexity of the tRNA world: mammalian tRNAs beyond protein synthesis. Nat. Rev. Mol. Cell Biol. *19*, 45–58.

Sievers, F., Wilm, A., Dineen, D., Gibson, T.J., Karplus, K., Li, W., Lopez, R., McWilliam, H., Remmert, M., Söding, J., et al. (2011). Fast, scalable generation of high-quality protein multiple sequence alignments using Clustal Omega. Mol. Syst. Biol. *7*, 539.

Slack, F.J. (2018). Tackling Tumors with Small RNAs Derived from Transfer RNA. N. Engl. J. Med. *378*, 1842–1843.

Spitale, R.C., Flynn, R.A., Zhang, Q.C., Crisalli, P., Lee, B., Jung, J.-W., Kuchelmeister, H.Y., Batista, P.J., Torre, E.A., Kool, E.T., and Chang, H.Y. (2015). Structural imprints *in vivo* decode RNA regulatory mechanisms. Nature *519*, 486–490.

Sulima, S.O., Hofman, I.J.F., De Keersmaecker, K., and Dinman, J.D. (2017). How Ribosomes Translate Cancer. Cancer Discov. *7*, 1069–1087.

Trapnell, C., Pachter, L., and Salzberg, S.L. (2009). TopHat: discovering splice junctions with RNA-Seq. Bioinformatics *25*, 1105–1111.

Valdmanis, P.N., Gu, S., Chu, K., Jin, L., Zhang, F., Munding, E.M., Zhang, Y., Huang, Y., Kutay, H., Ghoshal, K., et al. (2016). RNA interference-induced hepatotoxicity results from loss of the first synthesized isoform of microRNA-122 in mice. Nat. Med. *22*, 557–562.

Vogel, C., and Marcotte, E.M. (2012). Insights into the regulation of protein abundance from proteomic and transcriptomic analyses. Nat. Rev. Genet. *13*, 227–232.

Wang, Q., Lee, I., Ren, J., Ajay, S.S., Lee, Y.S., and Bao, X. (2013). Identification and functional characterization of tRNA-derived RNA

fragments (tRFs) in respiratory syncytial virus infection. Mol. Ther. *21*, 368–379.

Wilhelm, M., Schlegl, J., Hahne, H., Gholami, A.M., Lieberenz, M., Savitski, M.M., Ziegler, E., Butzmann, L., Gessulat, S., Marx, H., et al. (2014). Mass-spectrometry-based draft of the human proteome. Nature *509*, 582–587.

Yamasaki, S., Ivanov, P., Hu, G.-F., and Anderson, P. (2009). Angiogenin cleaves tRNA and promotes stress-induced translational repression. J. Cell Biol. *185*, 35–42.

Zhang, Y., Zhang, X., Shi, J., Tuorto, F., Li, X., Liu, Y., Liebers, R., Zhang, L., Qu, Y., Qian, J., et al. (2018). Dnmt2 mediates intergenerational transmission of paternally acquired metabolic disorders through sperm small non-coding RNAs. Nat. Cell Biol. *20*, 535–540.

Zhou, J., Liu, S., Chen, Y., Fu, Y., Silver, A.J., Hill, M.S., Lee, I., Lee, Y.S., and Bao, X. (2017). Identification of two novel functional tRNA-derived fragments induced in response to respiratory syncytial virus infection. J. Gen. Virol. *98*, 1600–1610.

STAR★METHODS

KEY RESOURCES TABLE

REAGENT or RESOURCE	SOURCE	IDENTIFIER
Antibodies		
Rabbit polyclonal anti-RPS28	Aviva systems biology	Cat# ARP65601_P050
Rabbit polyclonal anti-RPS7	Bethyl laboratories	Cat# A300-740A; RRID:AB_533451
Rabbit polyclonal anti-RPL35A	Bethyl laboratories	Cat# A305-106A; RRID:AB_2631501
Mouse monoclonal anti-GAPDH	Thermo Fisher	Cat# AM4300; RRID:AB_437392
Chemicals, Peptides, and Recombinant Proteins		
Cycloheximide	Sigma-Aldrich	Cat# C4859-1ML
Sodium arsenite	Sigma-Aldrich	Cat# 1062771000
Critical Commercial Assays		
Cell 96 Aqueous One Solution Cell Proliferation Assay (MTS)	Promega	Cat# G3582
Lipofectamine 2000	Thermo Fisher	Cat# 11668019
Superscript IV RT kit	Thermo Fisher	Cat# 12594100
TRIZOL reagent	Thermo Fisher	Cat# 15596026
Experimental Models: Cell Lines		
Mouse: Hepa 1-6 cells	ATCC	CRL-1830
Human: HeLa cells	ATCC	CCL-2
Oligonucleotides		
Anti-control: GtaCgCgGaaTaCTtC	Exiqon	N/A
Anti-Leu3′ts: tGTcAGgAgTggGaT	Exiqon	N/A
Anti-Leu3′tsMM: tCTcACgAgTggGaT	Exiqon	N/A
Anti-Leu3′tsMM2: tGTcAAgAcTggGaT	Exiqon	N/A
Northern probe for LeuCAG3′tsRNA: 5′-gtgtcagg agtgggattcg-3′	IDT	N/A
Northern probe for mouse ITS1: 5′-acgccgccgct cctccacagtctcccgtt-3′	IDT	N/A
Northern probe for mRNAs: See Table S3	IDT	N/A
Oligonucleotides for site-directed mutagenesis: See Table S4	IDT	N/A
Recombinant DNA		
CMV promoter-mouseRPS28 wt	This paper	N/A
CMV promoter-mouseRPS28 target-A mutant	This paper	N/A
CMV promoter-mouseRPS28 target-B mutant	This paper	N/A
CMV promoter-mouseRPS28 non-target mutant	This paper	N/A
Software and Algorithms		
RNA-hybrid program	Krüger and Rehmsmeier, 2006	https://bibiserv.cebitec.uni-bielefeld.de/rnahybrid
Mega software	Kumar et al., 2016b	https://www.megasoftware.net
MegAlign program	Burland, 2000	https://www.dnastar.com/software/molecular-biology/
PRISM 8.0	N/A	https://www.graphpad.com/
Integrative genomics viewer	Robinson et al., 2011	https://software.broadinstitute.org/software/igv/
Clustal Omega	Sievers et al., 2011	https://www.ebi.ac.uk/Tools/msa/clustalo/
TopHat2 (v.2.0.14)	Trapnell et al., 2009	https://ccb.jhu.edu/software/tophat/index.shtml

LEAD CONTACT AND MATERIALS AVAILABILITY

This study did not generate new unique reagents. Further information and requests for resources and reagents should be directed to and will be fulfilled by the corresponding author, Mark A. Kay (markay@stanford.edu).

EXPERIMENTAL MODEL AND SUBJECT DETAILS

Cell lines were grown at 37°C in 5% CO_2 humidified incubators. HeLa (human cervical cancer) and Hepa 1-6 (mouse hepatoma) cells were grown in DMEM medium containing 10% heat-inactivated fetal bovine serum (FBS), 2mM L-glutamine, 100 U/ml penicillin, and 100U/ml streptomycin.

METHOD DETAILS

Transfection

30-60 nM of locked nucleic acid (LNA) mixmers and/or plasmids were transfected using Lipofectamine 2000 (Thermo Fisher) according to the manufacturer's instructions. 700ng of the appropriate expression plasmid was transfected in 6 well dishes for RPS28 wt or mutant western blot analyses. Anti-sense oligonucleotides (DNA and LNA mixer) were synthesized by Exiqon. The siRPS28, siRPL7, siRPL35 and sicontrol were purchased from Dharmacon. DNA oligonucleotides were synthesized by IDT.

Oligonucleotides

All oligonucleotides used for cell viability experiments with inhibition of LeuCAG3′tsRNA and for detection of LeuCAG3′tsRNA and 18S rRNA precursors are listed in Key Resources Table. All PCR primers used for generation of northern probes to detect mRNAs are listed in Table S3.

Plasmid constructs

The full-length mouse *Rps28* gene was amplified from Hepa 1-6 cDNA with primers (5′-ctcgcgagagcgaaagtgag-3′ and 5′-taata taaatgctttatttaacagttgcag-3′) and was cloned into the pcDNA3.3 plasmid. Site-directed mutagenesis was performed with the QuikChange II XL Site-Directed Mutagenesis Kit (Stratagene) to generate point mutations or deletions in the recombinant *Rps28* gene. All oligonucleotides for site directed mutagenesis are listed in Table S4. All plasmid clones were confirmed by DNA sequencing.

Western blotting

24 h post-transfection, cell lysates were prepared using 1X cell lysis buffer (Cell Signaling) with 1 mM PMSF (Cell Signaling). 10-15 ug of protein lysate was run on 4%–12% SDS-PAGE and transferred to Hybond-P or nitrocellulose membrane (GE Healthcare). The membrane was incubated for 20 min at room temperature (RT) in Blocking Buffer (LI-COR Biosciences), washed, and incubated overnight (O/N) at 4°C with anti-RPS28 (1:1000, Aviva systems biology, ARP65601_P050), anti-RPS7 (1:1000, Bethyl laboratories, A300-740A), anti-RPL35A (1:1000, Bethyl laboratories, A305-106A) or anti-GAPDH antibodies (1:5000, Life Technologies, clone 6C5). After washing and incubation for 2 h at RT with secondary antibody (1:10,000, Fisher, 92568071 and 92532210), the protein signal was detected using Odyssey CLx imaging system (LI-COR Biosciences) according to the manufacturer's instructions.

Real time PCR

500 ng of total RNA was reverse transcribed with the superscript IV RT kit (Thermo Fisher) and subjected to gene expression analyses with gene-specific TaqMan probes (Mm99999915_g1 for *GAPDH* and Mm04203728_gH for mouse *Rps28*). Real time PCR was performed on a CFX384 Real-Time system (Bio-Rad).

RNA isolation and Northern blotting

Total RNA was isolated with TRIZOL reagent (Thermo Fisher) according to the manufacturer's instructions. Total RNA was resolved by electrophoresis on 15% (w/v) polyacrylamide gel with 7 M urea for detection of small RNAs less than 200 bp or on 0.9% agarose denaturating gel for detection of large RNAs (> 200 bp) followed by transfer onto a Hybond-N+ nylon membrane (Amersham). P32-labeled oligonucleotides or amplified cDNA probes were hybridized to the membrane in PerfectHyb Plus hybridization buffer (Sigma).

Polysome gradient and RNA preparation

Polysome gradient and RNA preparation were performed as described previously (Kim et al., 2017). 24 h post-transfection, cells were treated with 100 μg/ml of cycloheximide (Sigma) for 3min, were washed with cold DPBS (Sigma) containing 100 μg/ml of cycloheximide 2 times, and were lysed in buffer containing 15mM Tris–HCl (pH 7.5), 150mM KCl, 5mM $MgCl_2$, 500u/ml RNasin (Promega), and 1% Triton X-100 for 10 m. The lysates were cleared by centrifugation at 8,500 g-force for 5 m. For dissociation of 40S and

60S ribosomal subunit from ribosome, 200 ug/ml of Puromycin (Sigma-Aldrich, MO) was treated for 30 m before harvesting cells. Inhibition of translation initiation was performed as described previously (Ingolia et al., 2012). Cells were incubated with the 2 μg/ml harringtonine (Abcam) for 2 m or 1mM sodium arsenite (Fluka) for 1 h, followed by the treatment of cycloheximide before harvesting cells. The cleared lysates were loaded onto 10%–50% sucrose gradients (15 mM Tris–HCl (pH 7.5), 150mM KCl, 5 mM $MgCl_2$, 20u/ml SUPERaseIn (Thermo Fisher), and 100 μg/ml cycloheximide). Gradients were centrifuged at 35,000 rpm for 2 h 45 m in a SW41 rotor at 4°C and were collected into 14 tubes by pumping 70% sucrose into the bottom of the gradient and collecting from the top using a Teledyne Isco Foxy R1 Retriever/ UA-6 detector system with measurement of the absorbance at 254nm. Each obtained fractions were sequentially treated for 30 m at 37°C with 0.5 mg/ml proteinase K (New England Biolabs) in the presence of 5mM EDTA and 1% SDS. RNAs were extracted with an equal volume of phenol-chloroform-isoamylalcohol (25:24:1; Thermo Fisher), re-extracted with chloroform, and EtOH precipitation was performed.

The abundance of Rps28 transcript variants in mouse liver tissue

TopHat2 (v.2.0.14) (Trapnell et al., 2009) was used to align RNA sequence reads to the mouse mm9 genome. BAM files were visualized using the integrative genomics viewer (Robinson et al., 2011) and a Sashimi plot was generated to quantify the number of reads that mapped to splice junctions of each isoform of *Rps28*.

Structure probing of tsRNA targets and mouse Rps28 mRNA secondary structure prediction

The *in vivo* click selective 2′-hydroxyl acylation and profiling experiment (icSHAPE) generates the global view of RNA secondary structures in living cells for all four nucleotides. We retrieved RNA structure data from a previous study that probed nucleotide reactivity (i.e., single-strandedness) in mouse embryonic cells by using icSHAPE (Spitale et al., 2015). Mouse *Rps28* mRNA sequences were downloaded from NCBI RefSeq database (O'Leary et al., 2016) and the secondary structure was predicted using RNAStructure or RNAfold software by using default parameters, with and without icSHAPE data as constraints, respectively (Hofacker and Stadler, 2006; Reuter and Mathews, 2010). The secondary structure was visualized and edited using the VARNA program (Darty et al., 2009). Sequencing depth for icSHAPE is not adequate to obtain. icSHAPE scores for all mRNAs or in some instances the complete sequence of an individual mRNA.

tsRNA target prediction

LeuCAG3′tsRNA sequences of various species were obtained from the tRNA database (GtRNAdb) (Chan and Lowe, 2016) and the *RPS28* mRNA sequences were downloaded from the NCBI RefSeq database (O'Leary et al., 2016). The m.f.e. (minimal free energy) between the LeuCAG3′tsRNA and the binding site in the *RPS28* mRNA in various species was predicted using a RNA-hybrid program (Krüger and Rehmsmeier, 2006). The potential target sites were predicted using a −20 kcal/mol of energy threshold and three nucleotides loop constraints. The tsRNA binding predictions do not take into account nucleotide modifications.

Genetic distances of LeuCAG3′tsRNA

The genetic distances of LeuCAG3′tsRNA from various species can be measured by computing the proportion of nucleotide differences between each pair of sequences. The *p* genetic distances of all LeuCAG3′tsRNA sequences across different 44 species were calculated using MEGA software (Kumar et al., 2016b).

Percent identity

Percent identity is a quantitative measurement of the similarity between each pair of sequences. Closely related species are expected to have a higher percent identity for a given sequence than distantly related species, and thus percent identity to a degree reflects relatedness. The percent identity of LeuCAG3′tsRNA sequences across various species was calculated using the MegAlign program from DNASTAR software package (Burland, 2000).

Sequence alignment of RPS28 sequences

RPS28 mRNA sequences across different species were downloaded in FASTA format from NCBI (O'Leary et al., 2016). Then sequence alignment were conducted using Clustal Omega (Sievers et al., 2011).

Conservation analysis of LeuCAG3′tsRNA target site

The phyloP conservation scores of *RPS28* for 100 vertebrate species were downloaded from the UCSC Table Browser (Karolchik et al., 2004). The sites predicted to be conserved are assigned positive scores, while sites predicted to be tolerant to nucleotide changes are assigned negative scores. We calculated the average conservation score of each 22-nucleotides sliding window across the RPS28 CDS region and subsequently generated the conservation ranking for the LeuCAG3′tsRNA target site.

QUANTIFICATION AND STATISTICAL ANALYSIS

All data are presented as mean ± SD. Figure 2D (n = 3 independent experiments), Figure 3B (n = 4 independent experiments), Figure 3D (n = 3 independent experiments), and Figure 3F (n = 3 independent experiments) were analyzed by the two-tailed

Student's t test and Figure 2A (n = 4 independent experiments) was analyzed with one-way ANOVA using GraphPad Prism version 8.0.0 for Mac, GraphPad Software, San Diego, California USA, https://www.graphpad.com/. A *P value* of 0.05 or lower was considered significant.

DATA AND CODE AVAILABILITY

This study did not generate/analyze datasets/code.

Cell Reports, Volume *29*

Supplemental Information

A tRNA-Derived Small RNA Regulates Ribosomal Protein S28 Protein Levels after Translation Initiation in Humans and Mice

Hak Kyun Kim, Jianpeng Xu, Kirk Chu, Hyesuk Park, Hagoon Jang, Pan Li, Paul N. Valdmanis, Qiangfeng Cliff Zhang, and Mark A. Kay

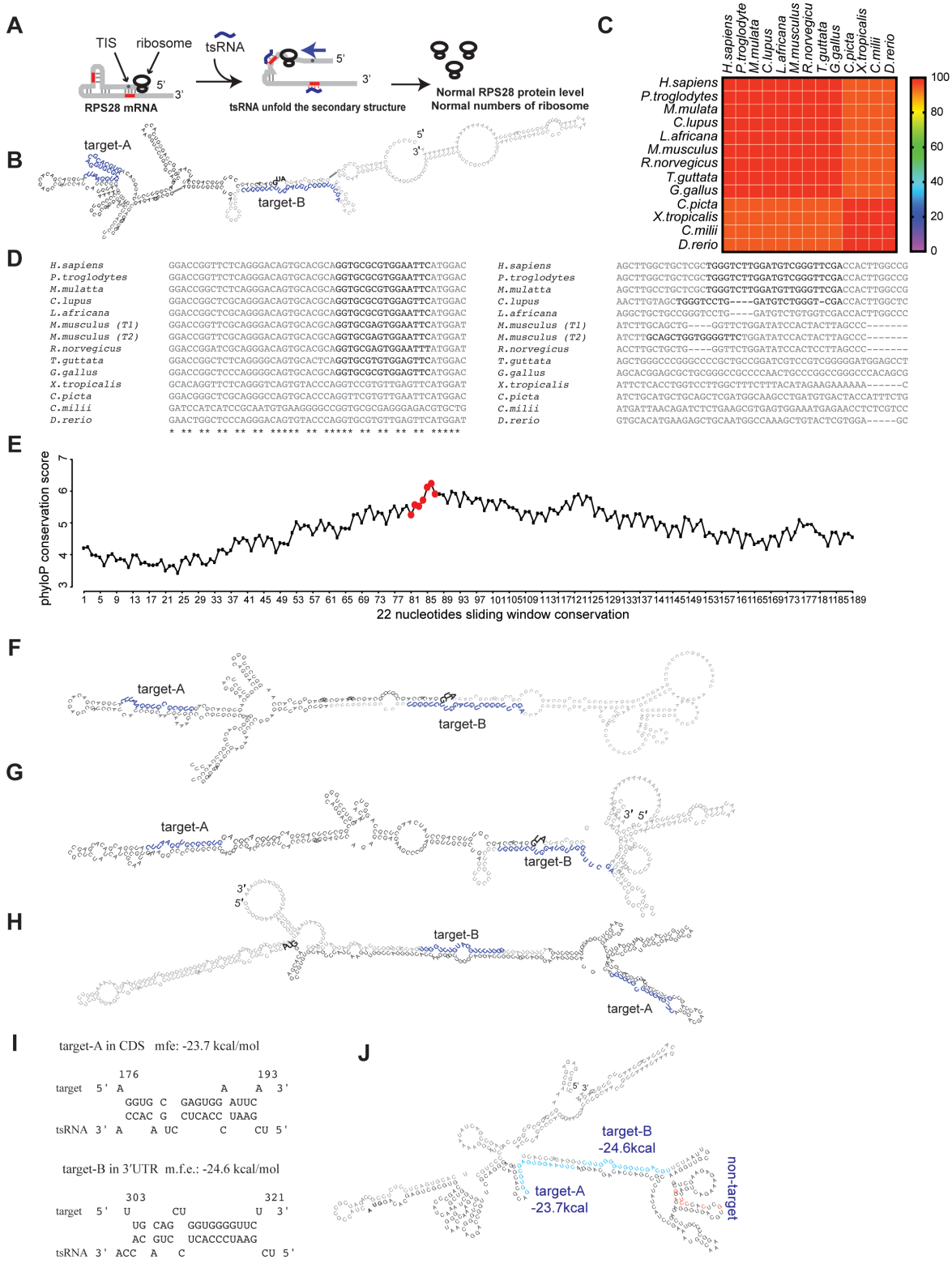
A
TIS
ribosome
tsRNA
5'
3'
RPS28 mRNA
tsRNA unfold the secondary structure
Normal RPS28 protein level
Normal numbers of ribosome
B
target-A
target-B
C
H.sapiens
P.troglodytes
M.mulata
C.lupus
L.africana
M.musculus
R.norvegicus
T.guttata
G.gallus
C.picta
X.tropicalis
C.milii
D.rerio
100
80
60
40
20
0
D
H.sapiens GGACCGGTTCTCAGGGACAGTGCACGCAGGTGCGCGTGGAATTCATGGAC
P.troglodytes GGACCGGTTCTCAGGGACAGTGCACGCAGGTGCGCGTGGAATTCATGGAC
M.mulatta GGACCGGCTCTCAGGGACAGTGCACGCAGGTGCGCGTGGAATTCATGGAC
C.lupus GGACCGGCTCGCAGGGACAGTGCACGCAGGTGCGCGTGGAGTTCATGGAC
L.africana GGACCGGCTCGCAGGGACAGTGCACGCAGGTGCGCGTGGAATTCATGGAC
M.musculus (T1) GGACCGGTTCGCAGGGACAGTGCACGCAGGTGCGAGTGGAATTCATGGAT
M.musculus (T2) GGACCGGTTCGCAGGGACAGTGCACGCAGGTGCGAGTGGAATTCATGGAT
R.norvegicus GGACCGGATCGCAGGGACAGTGCACGCAGGTGCGAGTGGAATTTATGGAT
T.guttata GGACCGGCTCTCAGGGGCAGTGCACTCAGGTGCGTGTGGAGTTCATGGAC
G.gallus GGACCGGCTCCCAGGGGCAGTGCACGCAGGTGCGCGTGGAGTTCATGGAC
X.tropicalis GCACAGGTTCTCAGGGTCAGTGTACCCAGGTCCGTGTTGAGTTCATGGAT
C.picta GGACGGGCTCGCAGGGCCAGTGCACCCAGGTTCGTGTTGAATTCATGGAC
C.milii GATCCATCATCCGCAATGTGAAGGGGCCGGTGCGCGAGGGAGACGTGCTG
D.rerio GAACTGGCTCCCAGGGACAGTGTACCCAGGTGCGTGTTGAGTTCATGGAT
H.sapiens AGCTTGGCTGCTCGCTGGGTCTTGGATGTCGGGTTCGACCACTTGGCCG
P.troglodytes AGCTTGGCTGCTCGCTGGGTCTTGGATGTCGGGTTCGACCACTTGGCCG
M.mulatta AGCTTGCCTGCTCGCTGGGTCTTGGATGTTGGGTTCGACCACTTGGCCG
C.lupus AACTTGTAGCTGGGTCCTG----GATGTCTGGGT-CGACCACTTGGCTC
L.africana AGGCTGCTGCCGGGTCCTG----GATGTCTGTGGTCGACCACTTGGCCC
M.musculus (T1) ATCTTGCAGCTG----GGTTCTGGATATCCACTACTTAGCCC-------
M.musculus (T2) ATCTTGCAGCTGGTGGGGTTCTGGATATCCACTACTTAGCCC-------
R.norvegicus ACCTTGCTGCTG----GGTTCTGGATATCCACTCCTTAGCCC-------
T.guttata AGCTGGGCCCGGGCCCCGCTGCCGGATCGTCCGTCGGGGGATGGAGCCT
G.gallus AGCACGGAGCGCTGCGGGGCCCGCCCCAACTGCCCGGCCGGGCCCACAGCG
X.tropicalis ATTCTCACCTGGTCCTTGGCTTTCTTTACATAGAAGAAAAAA------C
C.picta ATCTGCATGCTGCAGCTCGATGGCAAGCCTGATGTGACTACCATTTCTG
C.milii ATGATTAACAGATCTCTGAAGCGTGAGTGGAAATGAGAACCTCTCGTCC
D.rerio GTGCACATGAAGAGCTGCAATGGCCAAAGCTGTACTCGTGGA-----GC
E
phyloP conservation score
22 nucleotides sliding window conservation
F
target-A
target-B
G
target-A
target-B
3' 5'
H
3'
5'
target-B
target-A
I
target-A in CDS mfe: -23.7 kcal/mol
176 193
target 5' A A A 3'
GGUG C GAGUGG AUUC
CCAC G CUCACC UAAG
tsRNA 3' A A UC C CU 5'
target-B in 3'UTR m.f.e.: -24.6 kcal/mol
303 321
target 5' U CU U 3'
UG CAG GGUGGGGUUC
AC GUC UCACCCUAAG
tsRNA 3' ACC A C CU 5'
J
5' 3'
target-B
-24.6kcal
target-A
-23.7kcal
non-target

Figure S1. Related to Figure 1 – LeuCAG3′tsRNA and its target site in CDS of *RPS28* mRNA is conserved between vertebrate species. (A) Proposed model of LeuCAG3′tsRNA-mediated translation regulation in human cells (Kim et al., 2017). The LeuCAG3′tsRNA is processed from the mature Leu-CAG tRNA by an unknown process. It binds to two target sites (red colored region) in human *RPS28* mRNA and unwinds the secondary structure of the target sites during translation, maintaining a specific concentration of RPS28 protein and 40S ribosomes. **(B)** The detailed human *RPS28* mRNA (NM_001031.4) secondary structure is depicted. Grey, untranslated region (UTR); Black, coding sequences (CDS); Blue, the potential binding sites of the LeuCAG3′tsRNA. Translation initiation site (TIS) is indicated as black-bold characters. **(C)** The percent identity across 13 vertebrate species is depicted. Each percent identity is 95 or 100 demonstrating that LeuCAG3´tsRNA sequence is either identical or different by 1 nt between diverse vertebrate species. **(D)** The sequence alignments of target-A (left) and target-B sites (right) in *RPS28* mRNA for LeuCAG3′tsRNA across different species. The targets of LeuCAG3′tsRNA in *RPS28* mRNA of each species were predicted using RNAhybrid. *M. musculus* (T1) and (T2) are mouse *Rps28* transcript 1 and transcript 2, respectively. Black-colored nucleotides are the predicted target sites in each species. *, conserved site. **(E)** The average phyloP conservation score (y-axis) of each 22-nucleotide-long sliding window (x-axis) through the *RPS28* CDS across 100 vertebrate species. The red-colored consecutive seven, 22-nucleotide windows span the entire LeuCAG3′tsRNA target site. The average conservation score of a group of these seven windows is 5.75, which is the second highest score among those of all grouped consecutive seven, 22-nucleotide windows that span the whole *RPS28* CDS. (F, G, H) Schematic of the RPS28 mRNA secondary structure predicted by RNAfold. *P.troglodytes* RPS28 (XM_003953343.3) **(F)**. *M.mulatta* RPS28 (NM_001193436.1) **(G)**. *C.lupus* RPS28 (XM_542128.5) **(H)**. Grey, untranslated region (UTR); Black, coding sequences (CDS); Blue, the potential binding sites of the LeuCAG3´tsRNA. Translation initiation site (TIS) is indicated as black-bold characters. **(I)** The thermodynamic potential of LeuCAG3′tsRNA binding sites in the mouse *Rps28* mRNA: the target-A (nt 176 to 193) in the CDS and the target-B (nt 303 to 321) in the 3′ UTR. The binding site is predicted by RNAhybrid. Indicated numbers on each diagram represents the 5′ end and 3′ end position of the target site of the mouse *Rps*28 mRNA, respectively. **(J)** Schematic of the mouse *Rps28* mRNA (NM_001355384.1) secondary structure predicted by RNAfold. Blue, the possible binding sites of the LeuCAG3′tsRNA. Red, the altered nucleotides of the non-target RPS28 mutant.

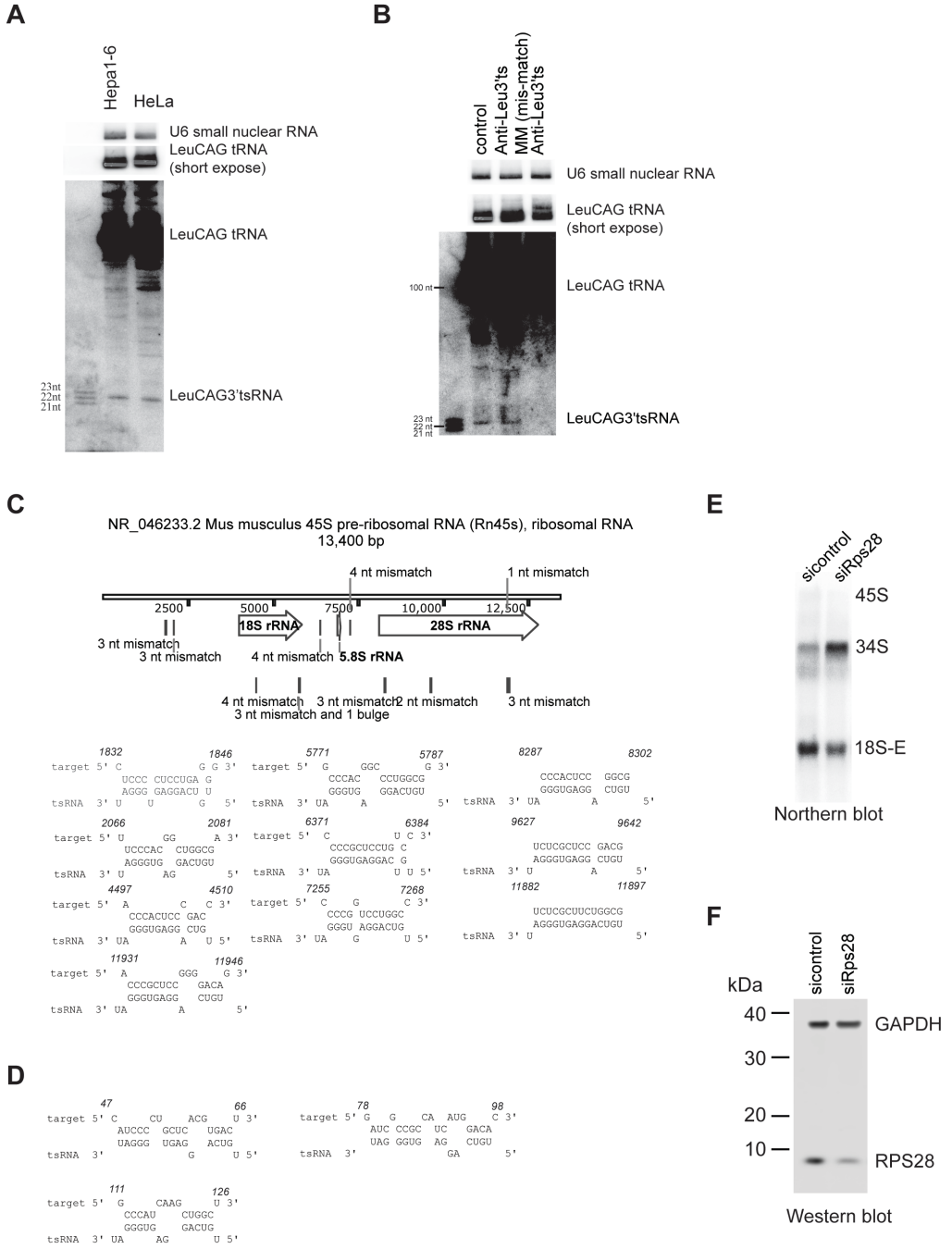
A
Hepa1-6
HeLa
U6 small nuclear RNA
LeuCAG tRNA
(short expose)
LeuCAG tRNA
23nt
22nt
21nt
LeuCAG3'tsRNA
B
control
Anti-Leu3'ts
MM (mis-match)
Anti-Leu3'ts
U6 small nuclear RNA
LeuCAG tRNA
(short expose)
100 nt
LeuCAG tRNA
23 nt
22 nt
21 nt
LeuCAG3'tsRNA
C
NR_046233.2 Mus musculus 45S pre-ribosomal RNA (Rn45s), ribosomal RNA
13,400 bp
4 nt mismatch
1 nt mismatch
2500
5000
7500
10,000
12,500
18S rRNA
28S rRNA
3 nt mismatch
3 nt mismatch
4 nt mismatch
5.8S rRNA
4 nt mismatch
3 nt mismatch and 1 bulge
3 nt mismatch
2 nt mismatch
3 nt mismatch
target 5' C G G 3'
UCCC CUCCUGA G
AGGG GAGGACU U
tsRNA 3' U U G 5'
1832
1846
target 5' G GGC G 3'
CCCAC CCUGGCG
GGGUG GGACUGU
tsRNA 3' UA A 5'
5771
5787
target 5' U GG A 3'
UCCCAC CUGGCG
AGGGUG GACUGU
tsRNA 3' U AG 5'
2066
2081
target 5' C U C 3'
CCCGCUCCUG C
GGGUGAGGAC G
tsRNA 3' UA U U 5'
6371
6384
target 5' A C C 3'
CCCACUCC GAC
GGGUGAGG CUG
tsRNA 3' UA A U 5'
4497
4510
target 5' C G C 3'
CCCG UCCUGGC
GGGU AGGACUG
tsRNA 3' UA G U 5'
7255
7268
target 5' A GGG G 3'
CCCGCUCC GACA
GGGUGAGG CUGU
tsRNA 3' UA A 5'
11931
11946
target 5' A C 3'
CCCACUCC GGCG
GGGUGAGG CUGU
tsRNA 3' UA A 5'
8287
8302
target 5' G C 3'
UCUCGCUCC GACG
AGGGUGAGG CUGU
tsRNA 3' U A 5'
9627
9642
target 5' U C 3'
UCUCGCUUCUGGCG
AGGGUGAGGACUGU
tsRNA 3' U 5'
11882
11897
D
target 5' C CU ACG U 3'
AUCCC GCUC UGAC
UAGGG UGAG ACUG
tsRNA 3' G U 5'
47
66
target 5' G G CA AUG C 3'
AUC CCGC UC GACA
UAG GGUG AG CUGU
tsRNA 3' GA 5'
78
98
target 5' G CAAG U 3'
CCCAU CUGGC
GGGUG GACUG
tsRNA 3' UA AG U 5'
111
126
E
sicontrol
siRps28
45S
34S
18S-E
Northern blot
F
kDa
sicontrol
siRps28
40
30
20
10
GAPDH
RPS28
Western blot

Figure S2. Related to Figure 2 – Antisense oligonucleotides targeting the LeuCAG3′tsRNA specifically inhibits the LeuCAG3′tsRNA and mouse RPS28 is required for ribosomal RNA processing in a mouse hepatoma cell line. (A) Total RNA was extracted from both cells and subjected to northern hybridization. The markers are synthesized oligonucleotides containing LeuCAG3′tsRNA sequences. U6 small nuclear RNA and LeuCAG tRNA are loading controls (n=2 independent experiments). **(B)** Northern analysis of the LeuCAG3′tsRNA and mature Leu-CAG tRNA post-transfection. The tsRNA (22 nt) and mature tRNA (around 100 nt) were detected with the same probe. To quantify and compare the relative amount of the mature tRNA, the blot was exposed for a shorter time after detecting the tsRNA (n=2 independent experiments). U6 snRNA and mature LeuCAG tRNA are the loading controls. **(C)** Schematic picture showing putative binding sites and binding structure of the anti-Leu3′ts ASO on the 45S primary transcript (45S pre-rRNA). To identify the tsRNA binding sites in the 45S pre-rRNA, we used the RNAhybrid program and 22-nt sequence from the 3′ end of LeuCAG-tRNA. The resulting two putative binding sites were positioned in the 5′ETS, two sites in 18S rRNA, one site in ITS1, one site in ITS2, and four sites in 28S rRNA, all of which have more than two mis-matches or a bulge except for the one binding site in 28S rRNA. The putative anti-Leu3′ts oligonucleotide binding site is indicated as a bar. **(D)** The potential interaction of Anti-LeuCAG3′tsRNA oligonucleotide and mouse *Rps28* mRNA: All of the potential interactions have more than two mis-matches. All binding sites were predicted by RNAhybrid. Indicated numbers on each diagram represents the 5′ end and 3′ end position of the target site on mouse 45S pre-rRNA or *Rps*28 mRNA, respectively. **(E, F)** Knockdown of the *Rps28* mRNA accumulated 34S pre-rRNA in Hepa 1-6 cells. Northern hybridization was performed with total RNA from Hepa 1-6 cells 24 h post-transfection (n=2 independent experiments). The ITS1 probe detects the 45S primary transcript and intermediate forms of the mature 18S rRNA including 34S, 29S, and 18S-E pre-rRNAs. The 47S and 29S pre-rRNAs are normally short-lived in cells due to their rapid processing. Mouse ribosomal RNA processing is depicted in Figure 2B **(E)**. The RPS28 protein level was measured by western blot 24 h post-transfection (n=2 independent experiments) **(F)**.

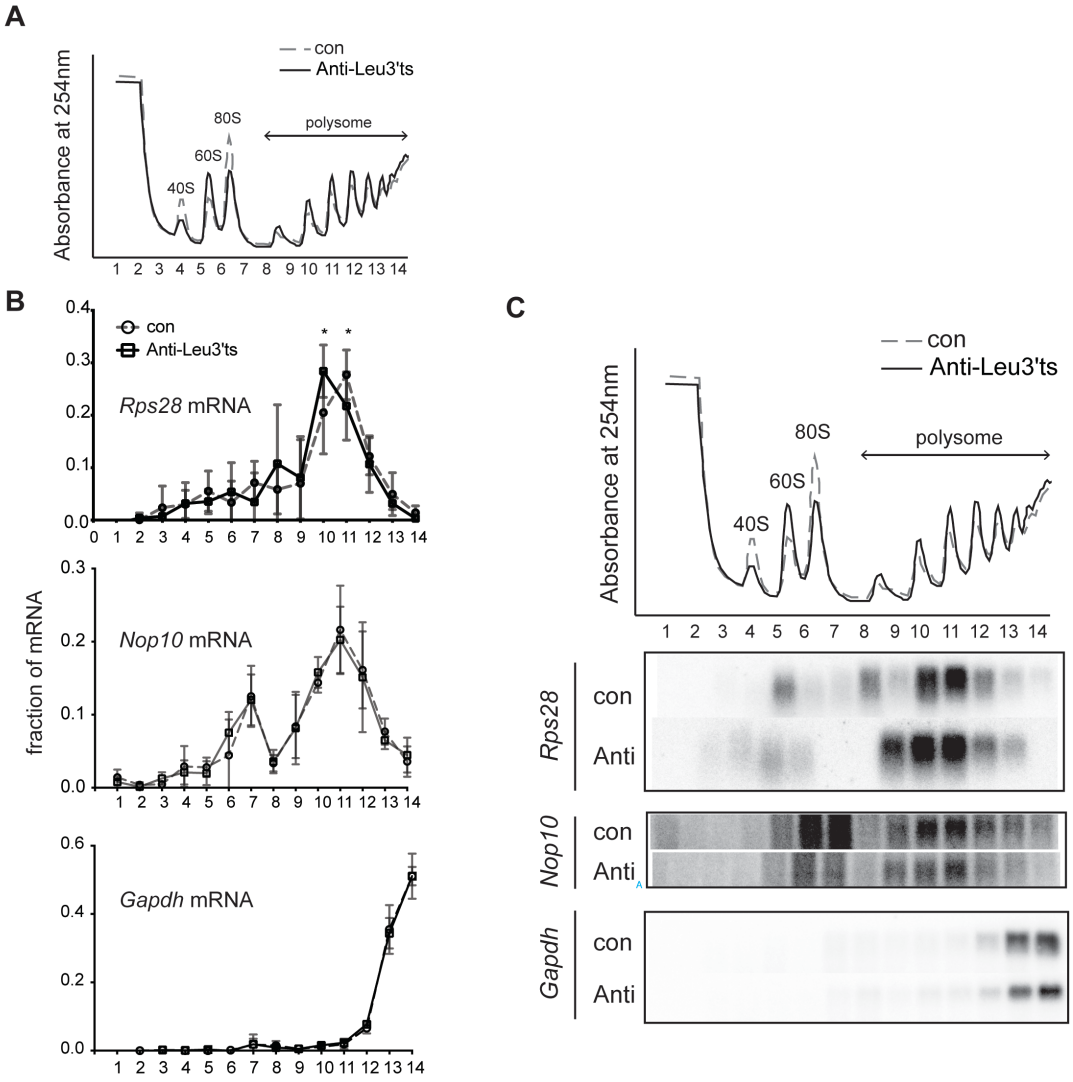

Figure S3. Related to Figure 3 – Inhibition of LeuCAG3′tsRNA reduced the number of ribosomes associated with *Rps28* mRNA, while *Nop10* and *Gapdh* mRNA were unaffected. Polysome analysis was performed using sucrose gradient fractionation 24 h post-transfection and subsequently northern hybridization was performed with the extracted RNA from each fraction (for *RPS28*, n=5 independent experiments; for *Nop10* and *GAPDH*, n=3 independent experiments). **(A)** Polysome profiles indicates the position of the 40S and 60S ribosomal free subunit, 80S monosome, and polysomes for each fraction. **(B)** Each fraction value for the specific mRNA was normalized to the sum of the mRNA level across all gradient fractions. **(C)** A represented northern image. X-axis, fraction number. con, control; Anti, Anti-LeuCAG3´tsRNA. The mean is indicated. Error bar, s.d. *, P<0.05 by two-tailed t-test.

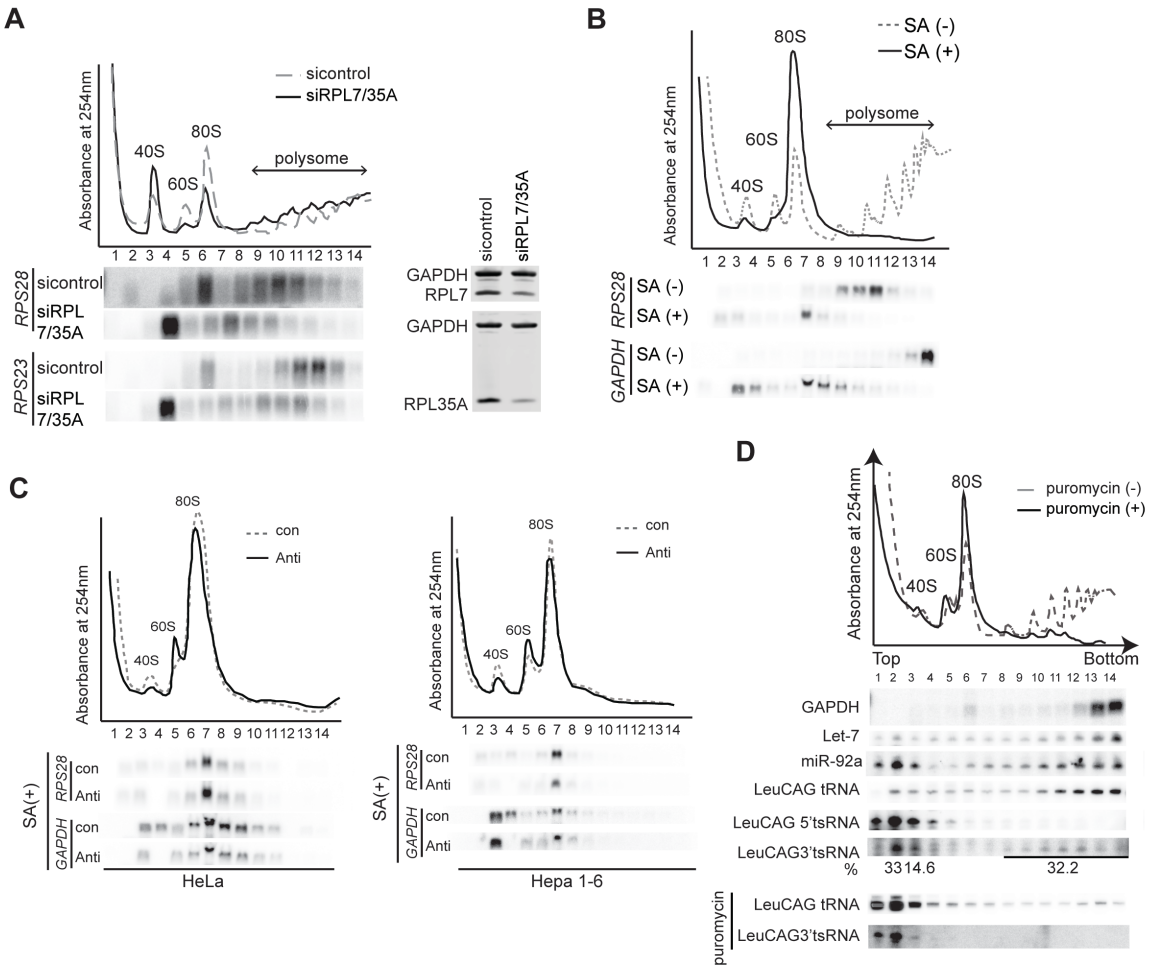

Figure S4. Related to Figure 4 – LeuCAG3´tsRNA regulates RPS28 post-translational initiation in both HeLa and Hepa 1-6 cells. The polysome profile (top) and northern hybridization (bottom) in each panel were analyzed 24 h post-transfection. The polysome profile indicates the position of ribosomal free subunit, monosome, and polysomes for each designated fraction and shows that the treatment with sodium arsenite (solid line) inhibits the formation of polysomes. **(A)** In HeLa cells, depletion of RPL7 and RPL35A, components of the 60S ribosome stalls RPS28 and RPS23 mRNA migration to fractions near the 40S subunit (n=2 independent experiments). Western blot showing depleted RPL7 and RPL35A protein levels by siRNA knockdown in the right panel. GAPDH is a loading control. **(B)** Sodium arsenite treatment stalls *RPS28* and *GAPDH* mRNA at the 80S monosome in HeLa cells (n=2 independent experiments). **(C)** Sodium arsenite treatment stalls RPS28 and GAPDH mRNA at the 80S monosome regardless of the inhibition of LeuCAG3´tsRNA in HeLa (left) and Hepa1-6 (right) cells (n=2 independent experiments). SA (+), treatment of sodium arsenite; SA (-), no treatment of sodium arsenite; con, control; Anti, Anti-LeuCAG3´tsRNA. **(D)** LeuCAG3´tsRNA co-migrates with polysomal fractions. Cytoplasmic lysates from HeLa cells were treated with cycloheximide or puromycin and separated by ultracentrifugation in 10−50% sucrose gradients. Total RNAs were extracted from each fraction, separated on a denaturing 15% acrylamide gel, and subjected to northern hybridization (n=2 independent experiments). Upper graph is the ribosomal profile detected at 254nm UV showing sucrose gradient fractionation discriminates the 40S and 60S ribosomal free subunits, 80S monosome, and polysomes. The percentage below the LeuCAG3´tsRNA northern result indicates the relative LeuCAG3´tsRNA abundance in fractions normalized to the sum of the LeuCAG3´tsRNA level across all gradient fractions.

sample	Transcript 1 (short form)	Transcript 2 (long form)	others	GEO accession number
liver_control_rep1		44	3	GSM1694991
liver_control_rep2		89		GSM1694992
liver_U6-sh-hAAT_25nt_rep1		52	2	GSM1694993
liver_U6-sh-hAAT_25nt_rep2		58		GSM1694994
liver_H1-sh-hAAT_25nt_rep1	1	43		GSM1694995
liver_H1-sh-hAAT_25nt_rep2		43		GSM1694996

Table S1. Related to Figure 1 – Relative expression of mouse *Rps28* transcript variants in whole liver. The number in each transcript column indicates the number of reads that span the splice junction (overlapping both exons).

NULL	NULL	NULL	NULL	NULL	NULL	NULL	NULL	NULL		
NULL	NULL	NULL	NULL	NULL	NULL	NULL	NULL	NULL		
NULL	NULL	NULL	NULL	NULL	NULL	NULL	NULL	NULL		
NULL	NULL	NULL	NULL	NULL	NULL	NULL	NULL	NULL		
NULL	NULL	NULL	NULL	NULL	NULL	NULL	NULL	NULL		
NULL	NULL	NULL	NULL	NULL	NULL	NULL	NULL	NULL		
NULL	NULL	NULL	NULL	NULL	NULL	NULL	NULL	NULL		
1.000	1.000	0.000	0.381	0.033	0.120	0.296	0.556	0.315	0.381	0.330
0.365	0.058	0.108	0.333	0.377	0.061	0.061	0.118	0.029	0.073	0.141
0.040	0.151	0.344	0.000	0.186	0.199	0.063	0.042	0.233	0.118	0.110
0.056	0.022	0.096	0.087	0.197	0.059	0.048	0.022	0.030	0.008	0.012
0.010	0.007	0.049	0.004	0.000	0.000	0.000	0.058	0.014	0.000	0.057
0.076	0.052	0.042	0.017	0.034	0.039	0.004	0.134	0.112	0.068	0.122
0.306	0.381	0.483	0.104	0.000	0.035	0.201	0.192	0.199	0.259	0.131
0.058	0.042	0.032	0.023	0.059	0.051	0.046	0.084	0.128	0.423	0.162
0.004	0.003	0.169	0.148	0.371	0.069	0.129	0.130	0.192	0.151	0.057
0.045	0.283	0.152	0.133	0.231	0.292	0.232	0.070	0.035	0.002	0.035
0.152	0.327	0.213	0.420	0.122	0.245	0.127	0.106	0.171	0.124	0.063
0.020	0.029	0.009	0.120	0.118	0.175	0.038	0.000	0.128	0.103	0.075
0.089	0.090	0.019	0.330	0.233	0.119	0.114	0.006	0.031	0.071	0.091
0.000	0.025	0.050	0.019	0.000	0.134	0.305	0.762	0.120	0.301	0.384
0.247	0.040	0.230	0.423	0.695	1.000	0.430	0.404	0.980	0.269	0.497
0.711	0.580	0.240	0.262	0.132	0.066	0.000	0.000	0.103	0.504	0.452
0.124	0.028	0.181	0.097	0.206	0.020	0.018	0.012	0.017	0.007	0.028
0.000	0.024	0.300	0.164	0.022	0.458	0.000	0.000	0.000	0.000	0.000
0.000	0.156	0.523	0.281	0.151	0.151	0.222	0.365	0.678	0.267	0.152
0.409	0.622	1.000	0.786	0.478	0.630	0.393	0.910	0.794	0.569	0.462
0.350	0.142	0.128	0.651	0.646	0.249	0.399	0.402	0.418	0.585	0.224
0.296	0.724	0.739	0.845	1.000	1.000	0.393	0.468	0.471	0.368	0.052
0.000	0.020	0.019	0.000	0.031	0.113	0.001	0.013	0.004	0.001	0.040
0.021	0.040	0.015	0.011	0.013	0.023	0.052	0.098	0.246	0.870	0.171
0.000	0.000	0.039	0.003	0.040	0.071	0.056	0.086	0.123	0.113	0.023
0.000	0.000	0.000	0.022	0.004	0.017	0.028	0.084	0.027	0.022	0.013
0.015	0.009	0.000	NULL	NULL	NULL	NULL	NULL	NULL	NULL	NULL
NULL	NULL	NULL	NULL	NULL	NULL	NULL	NULL	NULL	NULL	NULL
NULL	NULL	NULL	NULL	NULL	NULL	NULL	NULL	NULL	NULL	NULL

Table S2. Related to Figure 1 – icSHAPE scores for the full-length mouse *Rps28* transcript 2 (ENSMUST00000173844.7). Each number represents the scores for each nucleotide.

Human *GAPDH* mRNA: 5′-agatcatcagcaatgcctcct-3′ and 5′-tggtcatgagtccttccacg-3′	IDT	N/A
Human *RPS28* mRNA: 5′-gccgccatggacaccagccgtgtgc-3′ and 5′-tcagcgcaacctccgggcttc-3′	IDT	N/A
Human *RPS23* mRNA: 5′-gccgccatgggcaagtgtcgtggac-3′ and 5′-ttatgatcttggtctttccttc-3′	IDT	N/A
Mouse *Gapdh* mRNA: 5′-acccctcattgacctcaacta-3′ and 5′-cttctccatggtggtgaagac -3′	IDT	N/A
Mouse *Rps28*: 5′-ctcgcgagagcgaaagtgag-3′ and 5′-taatataaatgctttatttaacagttgcag-3′	IDT	N/A

Table S3. Related to STAR Methods – PCR primers used as northern probes for mRNAs.

Mouse *Rps28* target-A mutant: 5′-gagcggctggtgtcatccataaactcgaccctgacttgcgtgcactgtccctgcga-3′ and 5′-tcgcagggacagtgcacgcaagtcagggtcgagtttatggatgacaccagccgctc-3′	IDT	N/A
Mouse Rps28 target-B mutant: 5′-agagaagctcgaaggttgcgttaatcttggatatccactac-3′ and 5′-gtagtggatatccaagattaacgcaaccttcgagcttctct-3′	IDT	N/A
Mouse Rps28 non-target mutant: 5′-ttcgagcttctctttctgactgcagcaatgtcaggacgtcaccctctcgaacggggcc-3′ and 5′-ggccccgttcgagagggtgacgtcctgacattgctgcagtcagaaagagaagctcgaa-3′	IDT	N/A

Table S4. Related to STAR Methods – Oligonucleotides used for site-directed mutagenesis.